ligand to the heme iron and, possibly, electron transfer from Pdx to oxyP450cam to activate molecular oxygen.

The breakdown of oxyP450cam into the reaction products is a composite of several processes such as proton transfer, electron transfer, O−O bond cleavage, and oxygen transfer to the substrate. Thus, to fully understand the roles of the conformational changes on the P450cam monooxygenase system, further studies on the effects of Pdx on each partial reaction and on the structure of the oxyP450cam/Pdx complex are necessary.

ACKNOWLEDGMENT

The authors thank Prof. Thomas L. Poulos and Dr. Bhaskar for helpful comments and Ms. Yoko Toba for her excellent technical assistance.

REFERENCES

1. Katagiri, M., Ganguli, B. N., and Gunsalus, I. C. (1968) *J. Biol. Chem. 243*, 3543−3546.
2. Gunsalus, I. C., Meeks, J. R., Lipscomb, J. D., Debrunner, P., and Munck, E. (1974) in *Molecular Mechanisms of Oxygen Activation* (Hayaishi, O., Ed.) pp 559−613, Academic Press, New York.
3. Shimada, H., Sligar, S. G., Yoem, H., and Ishimura, Y. (1997) in *Oxygenase and Model System* (Funabiki, T., Ed.) pp 195−221, Kluwer Academic Publisher, London.
4. Kimata, Y., Shimada, H., Hirose, T., and Ishimura, Y. (1995) *Biochem. Biophys. Res. Commun. 208*, 96−102.
5. Hishiki, T., Shimada, H., Nagano, S., Egawa, T., Kanamori, Y., Makino, R., Park, S. Y., Adachi, S., Shiro, Y., and Ishimura, Y. (2000) *J. Biochem. (Tokyo) 128*, 965−974.
6. Gerber, N. C., and Sligar, S. G. (1994) *J. Biol. Chem. 269*, 4260−4266.
7. Gerber, N. C., and Sligar, S. G. (1992) *J. Am. Chem. Soc. 114*, 8742−8743.
8. Lipscomb, J. D., Sligar, S. G., Namtvedt, M. J., and Gunsalus, I. C. (1976) *J. Biol. Chem. 251*, 1116−1124.
9. Shiro, Y., Iizuka, T., Makino, R., Ishimura, Y., and Morishima, I. (1989) *J. Am. Chem. Soc. 111*, 7707−7711.
10. Pochapsky, S. S., Pochapsky, T. C., and Wei, J. W. (2003) *Biochemistry 42*, 5649−5656.
11. Tosha, T., Yoshioka, S., Takahashi, S., Ishimori, K., Shimada, H., and Morishima, I. (2003) *J. Biol. Chem. 278*, 39809−39821.
12. Lipscomb, J. D. (1980) *Biochemistry 19*, 3590−3599.
13. Ishimura, Y., Makino, R., Iizuka, T., and Shimada, H. (1987) in *Cytochrome P450: New Trends* (Sato, R., Omura, T., Imai, Y., and Fujii-Kuriyama, Y., Eds.) pp 151, Yamada Science Foundation, Nara.
14. Unno, M., Christian, J. F., Benson, D. E., Gerber, N. C., Sligar, S. G., and Champion, P. M. (1997) *J. Am. Chem. Soc. 119*, 6614−6620.
15. Unno, M., Christian, J. F., Sjodin, T., Benson, D. E., Macdonald, I. D., Sligar, S. G., and Champion, P. M. (2002) *J. Biol. Chem. 277*, 2547−2553.
16. Pochapsky, T. C., Lyons, T. A., Kazanis, S., Arakaki, T., and Ratnaswamy, G. (1996) *Biochimie 78*, 723−733.
17. Kramer, W., Drutsa, V., Jansen, H. W., Kramer, B., Pflugfelder, M., and Fritz, H. J. (1984) *Nucleic Acids Res. 12*, 9441−9456.
18. Imai, M., Shimada, H., Watanabe, Y., Matsushima-Hibiya, Y., Makino, R., Koga, H., Horiuchi, T., and Ishimura, Y. (1989) *Proc. Natl. Acad. Sci. U.S.A. 86*, 7823−7827.
19. Gunsalus, I. C., and Wagner, G. C. (1978) *Methods Enzymol. 52*, 166−188.
20. Unno, M., Shimada, H., Toba, Y., Makino, R., and Ishimura, Y. (1996) *J. Biol. Chem. 271*, 17869−17874.
21. Brewer, C. B., and Peterson, J. A. (1986) *Arch. Biochem. Biophys. 249*, 515−521.
22. Harris, T. K., Davidson, V. L., Chen, L., Mathews, F. S., and Xia, Z. X. (1994) *Biochemistry 33*, 12600−12608.
23. Schulze, H., Ristau, O., and Jung, C. (1994) *Eur. J. Biochem. 224*, 1047−1055.
24. Caughey, W. S., Shimada, H., Choc, M. G., and Tucker, M. P. (1981) *Proc. Natl. Acad. Sci. U.S.A. 78*, 2903−2907.
25. Poulos, T. L., Perez, M., and Wagner, G. C. (1982) *J. Biol. Chem. 257*, 10427−10429.
26. Koga, H., Sagara, Y., Yaoi, T., Tsujimura, M., Nakamura, K., Sekimizu, K., Makino, R., Shimada, H., Ishimura, Y., Yura, K., Go, M., Ikeguchi, M., and Horiuchi, T. (1993) *FEBS Lett. 331*, 109−113.
27. Nakamura, K., Horiuchi, T., Yasukochi, T., Sekimizu, K., Hara, T., and Sagara, Y. (1994) *Biochim. Biophys. Acta 1207*, 40−48.
28. Jung, C., Hoa, G. H., Schroder, K. L., Simon, M., and Doucet, J. P. (1992) *Biochemistry 31*, 12855−12862.
29. O'Keefe, D. H., Ebel, R. E., Peterson, J. A., Maxwell, J. C., and Caughey, W. S. (1978) *Biochemistry 17*, 5845−5852.
30. Ray, G. B., Li, X. Y., Ibers, J. A., Sessler, J. L., and Spiro, T. G. (1994) *J. Am. Chem. Soc. 116*, 162−172.
31. Legrand, N., Bondon, A., Simonneaux, G., Jung, C., and Gill, E. (1995) *FEBS Lett. 364*, 152−156.
32. Sjodin, T., Christian, J. F., Macdonald, I. D., Davydov, R., Unno, M., Sligar, S. G., Hoffman, B. M., and Champion, P. M. (2001) *Biochemistry 40*, 6852−6859.
33. Makino, R., Iizuka, T., Ishimura, Y., Uno, T., Nishimura, Y., and Tsuboi, M. (1984) in *Ninth International Conference on Raman Spectroscopy*, pp 492−493, Chemical Society of Japan, Tokyo.
34. Holden, M., Mayhew, M., Bunk, D., Roitberg, A., and Vilker, V. (1997) *J. Biol. Chem. 272*, 21720−21725.
35. Shimada, H., Nagano, S., Ariga, Y., Unno, M., Egawa, T., Hishiki, T., Ishimura, Y., Masuya, F., Obata, T., and Hori, H. (1999) *J. Biol. Chem. 274*, 9363−9369.
36. Yoshioka, S., Tosha, T., Takahashi, S., Ishimori, K., Hori, H., and Morishima, I. (2002) *J. Am. Chem. Soc. 124*, 14571−14579.
37. Yoshioka, S., Takahashi, S., Ishimori, K., and Morishima, I. (2000) *J. Inorg. Biochem. 81*, 141−151.
38. Furukawa, Y., and Morishima, I. (2001) *J. Biol. Chem. 276*, 12983−12990.
39. Ivkovic-Jensen, M. M., and Kostic, N. M. (1996) *Biochemistry 35*, 15095−15106.
40. Kraulis, P. J. (1991) *J. Appl. Crystallogr. 24*, 946−950.
41. Merritt, E. A., and Murphy, M. E. P. (1994) *Acta Crystallogr. D 50*, 869−873.
42. DeLano, W. L. (2002), DeLano Scientific, San Carlos, CA.

BI035410P

THE JOURNAL OF BIOLOGICAL CHEMISTRY
Vol. 278, No. 43, Issue of October 24, pp. 41597–41606, 2003
Printed in U.S.A.

Kinetic and Spectroscopic Characterization of a Hydroperoxy Compound in the Reaction of Native Myoglobin with Hydrogen Peroxide*

Received for publication, October 10, 2002, and in revised form, August 4, 2003
Published, JBC Papers in Press, August 5, 2003, DOI 10.1074/jbc.M210383200

Tsuyoshi Egawa‡§, Shiro Yoshioka¶‖, Satoshi Takahashi¶, Hiroshi Hori‡‡, Shingo Nagano‡, Hideo Shimada‡, Koichiro Ishimori¶, Isao Morishima¶, Makoto Suematsu‡, and Yuzuru Ishimura‡§§**

From the ‡Department of Biochemistry, School of Medicine, Keio University, Shinanomachi, Shinjuku-ku, Tokyo 160-8582, the ¶Department of Molecular Engineering, Graduate School of Engineering, Kyoto University, Kyoto 606-8501, and the ‡‡Division of Biophysical Engineering, Graduate School of Engineering Science, Osaka University, Toyonaka, Osaka 560-8531, Japan

The reaction of metmyoglobin with H_2O_2 was investigated in a pH range between 8.5 and 6.0 with the aid of stopped flow-rapid scan and rapid freezing-EPR techniques. Singular value decomposition analyses of the stopped flow data at pH 8.5 revealed that a spectral species previously unknown accumulated during the reaction and exhibited a Soret absorption maximum at ≥423 nm. In the EPR experiments, the new species exhibited a set of g values at 2.32, 2.19, and 1.94, indicating that the species was assignable to a ferric hydroperoxy (Fe(III)[O–O–H]$^-$) compound. In contrast, the hydroperoxy compound scarcely accumulated in the reaction at pH 6.0, and the dominant intermediate species accumulated was compound I, which was derived from the oxygen-oxygen bond cleavage of the hydroperoxy compound. The accumulated amount of the hydroperoxy compound relative to compound I showed a pH dependence with an apparent pK_a (pK_a^{app}) from 6.95 to 7.27 depending on the metmyoglobins examined. This variation in pK_a^{app} paralleled that in pK_a of the acid-alkaline transition (pK_a^{AB}) of metmyoglobins, suggesting that the accumulation of hydroperoxy compound is controlled by the distal histidine. We propose that the H_2O_2 activation by metmyoglobin is promoted at the acidic condition due to the imidazolium form of the distal histidine, and we further propose that the controlled protonation state of the distal histidine is important for the facile O–O bond cleavage in heme peroxidases.

A large number of heme enzymes catalyze heterolysis of hydrogen peroxide (H_2O_2)[1] and utilize H_2O_2 as a source of oxidizing equivalents for biological oxidative reactions. The enzymes include a family of heme peroxidases from plants, yeast, fungi, and mammals (1–6), soybean peroxygenase (7), and bacterial and fungal catalase peroxidases (8–10). High valent intermediates such as compounds I and II, which possess an oxoferryl porphyrin π-cation radical (Por^+-Fe(IV)[O]$^{2-}$, where Por^+ represents porphyrin π-cation radical) and an oxyferryl heme (Por-Fe(IV)[O]$^{2-}$), respectively, are known to be created upon the reaction of the heme enzymes with H_2O_2 and to carry out various oxidation reactions (1–4). Compound I is the first detectable intermediate in the reactions of the heme enzymes previously studied, and the subsequent one-electron reduction of compound I by the substrate generates compound II (1–4). In some enzymes such as cytochrome *c* peroxidase (CcP), the oxidizing equivalent on the π-cation heme of compound I is rapidly transferred to an amino acid residue in the protein moiety, creating another type of compound I (CcP-type compound I), which oxidizes the substrates (2). The chemical and enzymatic properties of the reaction between ferric heme and H_2O_2 have attracted considerable research interests to understand the reaction mechanisms of the heme enzymes.

As an approach to the above-mentioned research interest, investigations on the reaction between myoglobin (Mb) and H_2O_2 have long been made by several groups (11–19). Mb is a single domain heme protein that primarily serves as an oxygen storage compound using the ferrous state of the heme. The ferric form of Mb (metMb) is known to be capable of reacting with H_2O_2, forms an analog of the porphyrin π-cation-type compound I (11), and also forms that of CcP-type compound I (12–14). Both analogs can oxidize organic compounds (11, 15–19). The latter analog is termed ferryl Mb, whereas the former one, which was found recently (11), is named myoglobin compound I. All the basic reactions catalyzed by heme enzymes, *i.e.* formation of compound I, intramolecular electron transfer from an aromatic amino acid residue to the heme of compound I, and oxidation of organic or inorganic compounds by the high valent species, can be observed in Mb (11, 15–19). In this context, the reaction between H_2O_2 and metMb has been considered as a model system to understand the activation mechanisms of H_2O_2 by heme enzymes (11, 15, 18, 19).

Chemical properties of the high valent species and mechanisms of reaction steps after formation of compound I have

* This work was supported in part by grant-in-aids for scientific research on priority areas from the Ministry of Education, Science, and Culture of Japan, by the Special Coordination Funds of the Science and Technology Agency of Japan, by Japan-United States Cooperative Science Program, and by grants from Keio University. The costs of publication of this article were defrayed in part by the payment of page charges. This article must therefore be hereby marked "*advertisement*" in accordance with 18 U.S.C. Section 1734 solely to indicate this fact.

§ To whom correspondence should be addressed: Dept. of Biochemistry, School of Medicine, Keio University, 35 Shinanomachi, Shinjuku-ku, Tokyo 160-8582, Japan. Tel.: 81-3-3353-1997; Fax: 81-3-3358-8138; E-mail: egawa@sc.itc.keio.ac.jp.

‖ Present address: Dept. of Biochemistry, Vanderbilt University School of Medicine, Nashville, TN 37232-0146.

** Present address: Division of Physical Chemistry, Institute for Protein Research, Osaka University, Suita-shi, Osaka 565-0871, Japan.

§§ Present address: Dept. of Biochemistry, the University of Texas Health Science Center, San Antonio, TX 78229-3900.

[1] The abbreviations used are: H_2O_2, hydrogen peroxide; metMb, metmyoglobin; ferryl Mb, ferryl myoglobin; CcP, cytochrome *c* peroxidase; HRP, horseradish peroxidase; LiP, lignin peroxidase; SVD, singular value decomposition.

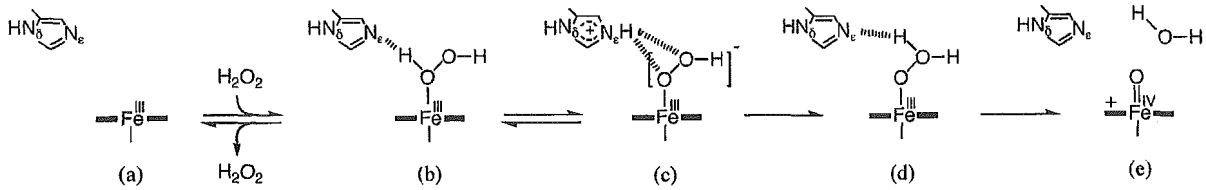

FIG. 1. **Hypothetical mechanism for compound I formation.** The reaction scheme (*steps a–e*) is drawn on the basis of Poulos and Kraut (26). *Broken lines* represent hydrogen bonds.

been studied extensively for peroxidases (1–6) and also for Mb (11, 15–19). On the other hand, mechanisms for compound I formation from ferric heme and H_2O_2 in heme proteins are still under debate (20–25). For compound I formation, Poulos and Kraut (26) proposed essential roles of a histidine residue at the distal vicinity of the heme, the distal histidine, which is highly conserved in peroxidases (26) and Mb (27). Based on their proposal, and also on results of recent quantum chemical studies (20–22), the catalysis of H_2O_2 by peroxidase has been supposed to proceed as shown in Fig. 1: *a* and *b*, H_2O_2 coordinates to ferric heme; *c*, the distal histidine then abstracts a proton from H_2O_2 (base catalysis), producing a hydroperoxy anion species (Fe(III)[O–O–H]$^-$); *d* and *e*, the protonated form (imidazolium form) of the distal histidine donates its proton back to the terminal oxygen of the hydroperoxy group (acid catalysis) to assist the heterolytic oxygen-oxygen (O–O) bond cleavage, leading to the formation of compound I.

Site-directed mutagenesis has demonstrated the importance of the distal histidine in peroxidases; an aliphatic amino acid substitution leads to a significant decrease in the rate of formation of compound I (28–31). However, identification and characterization of the postulated intermediates as discernible entities were not successful. Up to now, stopped flow observations about intermediates, which form prior to compound I, upon adding H_2O_2 to peroxidases have only been reported for horseradish peroxidase (HRP). These studies were done on reactions of HRP with H_2O_2 in either 50% methanol or 100% chlorobenzene at subzero temperature (32, 33). It is, however, unknown whether the reactions in organic solvents are identical to those under physiological conditions. The properties of the above precursors are also unclear, because characterizations by physicochemical techniques such as EPR and electron nuclear double resonance spectroscopies were not applied.

On the other hand, studies employing cryoradiolytic reductions of oxy hemes have succeeded in EPR and/or ENDOR characterizations of Fe(III)[O–O–H]$^-$ hemes formed in heme proteins including hemoglobin (34–36), myoglobin (34, 35), cytochrome P450 (37), heme oxygenase (36), and HRP (35, 38). These studies have indicated that the Fe(III)[O–O–H]$^-$ species are low spin. Indeed, optical absorption spectra of Fe(III)-[O–O–H]$^-$ species (λ_{max}, ~420 nm) are typical of ferric low spin hemes (38, 39), and they are different from any reported spectra by the stopped flow studies described above. Therefore, in order to investigate the molecular mechanism of compound I formation and the functions of the distal histidine, it is necessary to examine whether the Fe(III)[O–O–H]$^-$ species characterized by the oxy heme reduction studies are also involved in the reactions of H_2O_2 and ferric heme proteins having the histidine. For HRP, however, a recent study indicated that compound I formation is complete within a very short time (~200 μs) at ambient temperature in aqueous buffers, and identification of any precursor of compound I was difficult (40).

In order to address the above problem, and also to give insights into the roles of amino acid residues that form the heme pockets of heme enzymes, we followed the reaction between H_2O_2 and metMb in detail. By using stopped flow-rapid scan, singular value decomposition (SVD), and rapid freezing-EPR techniques, we succeeded in detecting a hydroperoxy anion compound (Fe(III)[O–O–H]$^-$) that is closely related to one of the postulated intermediates in the peroxidase reactions. Analyses of population changes of the hydroperoxy compound and compound I as a function of pH clearly demonstrated the involvement of the distal histidine in the reaction. Based on the present findings, we postulated mechanisms for the reaction between metMb and H_2O_2, and we also discussed the reaction mechanisms of the heme peroxidases.

EXPERIMENTAL PROCEDURES

Materials—Sperm whale and horse heart metMbs were purchased from Sigma. Human metMb and its T67N mutant were expressed in *Escherichia coli* and were purified as described elsewhere (18, 41). Each metMb dissolved in a potassium phosphate buffer was treated with a small amount of potassium ferricyanide as described previously (11) to eliminate the reduced form of Mb remaining in the commercial products or in the preparations extracted from *E. coli*. The oxidized proteins were extensively dialyzed and further purified by CM-cellulose column chromatography (11).

Stopped Flow-Rapid Scan Spectrophotometry—Changes in the optical absorption were measured by using an RSP-601 stopped flow-rapid scan spectrophotometer (UNISOKU Co., Ltd., Osaka, Japan) (11, 42). The instrumental dead time was estimated to be ~5 ms by employing a pseudo first-order reaction of 2,6-dichlorophenolindophenol with ascorbic acid (43).

Singular Value Decomposition—Time-resolved absorption spectra, which were obtained by using the stopped flow-rapid scan spectrophotometer, were analyzed by the technique of SVD (11, 42, 44–48). In the present investigation, the rapid scan spectroscopic system allowed us to record absorption data at up to 512 points for both wavelength and time, and hence 512 × 512 data points were obtained upon each run of the stopped flow experiments. We collected data from 19 experimental runs and averaged them. Among the data thus obtained, those at every 1.62 nm from 322 to 525 nm (126 data points) and at every 3 ms from 6 to 195 ms (64 spectral scans) were selected. This time range was selected in order to cover most of the reaction period under the present experimental conditions. The data set of 126 × 64 points thus obtained was subjected to the SVD calculation. The computer program used for the calculation was described elsewhere (11, 42).

Kinetic Parameters in Three Component Reactions—Concentrations of chemical species in three component sequential reaction represented by Reaction 1 are by Equations 1 and 2,

$$R \xrightarrow{k_1} I \xrightarrow{k_2} P$$

REACTION 1

$$[R] = [R]_0 \exp(-k_1 t) \qquad \text{(Eq. 1)}$$

$$[I] = [R]_0 \frac{k_1}{k_2 - k_1} \{\exp(-k_1 t) - \exp(-k_2 t)\} \qquad \text{(Eq. 2)}$$

where k_1 and k_2 are rate constants of the reaction, and $[R]_0$ is the initial concentration of the reactant (R) (49). Integrating Equations 1 and 2 with respect to time (t) from 0 to ∞, we obtained equations for total accumulated amounts of R and I in Reaction 1, and their ratio is given by Equation 3,

$$[I]_{total}/[R]_{total} = k_1/k_2 \qquad \text{(Eq. 3)}$$

On the other hand, the equation used for determining maximum accumulation time (t_{max}; time at which concentration reaches the maximum

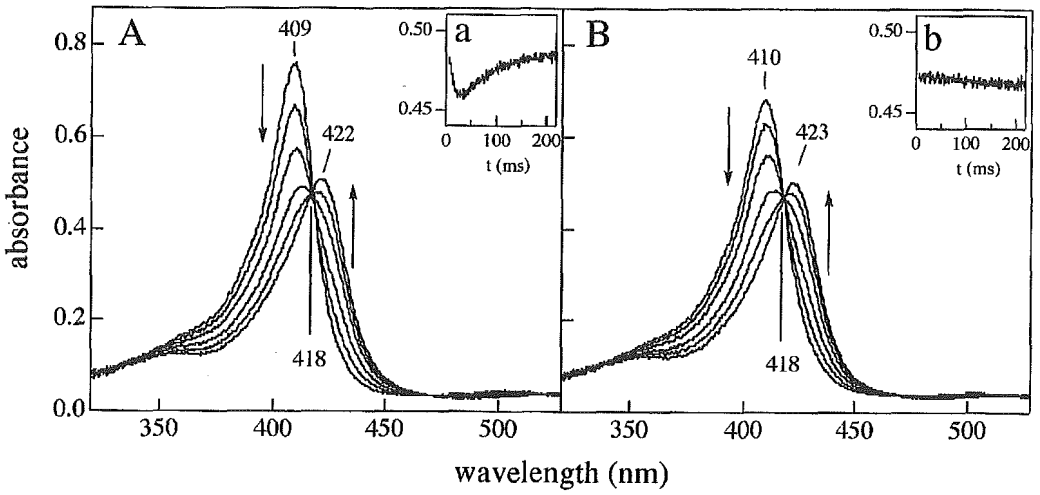

FIG. 2. **Absorption changes of the reaction of 5 μM sperm whale metMb with 50 mM H_2O_2 at pH 6.0 (*A*) and 8.5 (*B*).** Absorption spectra in both *A* and *B* were recorded at 6, 15, 30, 60, 100, and 200 ms after starting the reaction by the stopped flow-rapid scan system. *Arrows* indicate the directions of the absorption changes. Time profiles of absorption changes were followed at 418 nm (*insets a* and *b*). Buffer systems used were 200 mM potassium phosphate and 200 mM glycylglycine-NaOH at pH 6.0 and 8.5, respectively. All measurements were carried out at 25 °C.

value) of intermediate *I* in Reaction 1 is found in Ref. 49 as shown in Equation 4,

$$t_{max} = \frac{1}{k_2 - k_1} \ln \frac{k_2}{k_1} \qquad \text{(Eq. 4)}$$

Rapid Freezing-EPR Spectroscopy—Samples for EPR measurements were prepared by using a recently developed rapid freezing apparatus that was composed of a rapid mixing chamber and a freeze-quench device. The details of this apparatus are described elsewhere (40). We mixed metMb (1 mM) and H_2O_2 (200 mM) solutions in a 1:1 ratio and rapidly froze the mixed solution at 77 K to obtain the frozen flakes. The frozen flakes were collected and transferred into an EPR tube, and the EPR spectra of the samples were recorded at 15 K. The freezing dead time (time period from mixing to complete quenching) of our apparatus is 200 μs at minimum and is changeable by arranging conditions such as mixing flow rate and distance between the mixing and freeze-quench devices (40). Methods to calibrate the dead time were described already (40). In the present experiments, the freezing dead time was fixed at ~3 ms. EPR spectra were measured by a Varian E-12 spectrometer equipped with an Oxford ESR-900 liquid helium cryostat. Measurements were carried out at the X-band (9.22 GHz) microwave frequency.

RESULTS

Changes in Absorption Spectra during the Reaction between metMb and H_2O_2—Fig. 2*A* shows spectral changes observed during the reaction of 5 μM sperm whale metMb with 50 mM H_2O_2 in 200 mM potassium phosphate buffer, pH 6.0. The spectral changes shown here well reproduce those we reported previously for the same reaction (11). As we already indicated, formation of myoglobin compound I is detectable under the above experimental conditions (11). Although these spectral changes might be viewed as an apparently single process of conversion from metMb (λ_{max}, 409 nm) to ferryl Mb (λ_{max}, 422 nm), the time profile of the absorption at an isosbestic point (418 nm) between the spectra of metMb and ferryl Mb shows formation of an intermediate (Fig. 2, *inset a*). The temporary decrease in the time profile is caused by the accumulation of compound I in the reaction system (11). This accumulation of compound I can be observed more clearly in D_2O (at pD 6.0) (11).

In the present study, we show that the kinetics of the above reaction depends on the pH. Fig. 2*B* shows the absorption changes of the reaction at pH 8.5 in 200 mM glycylglycine-NaOH buffer. The reaction conditions other than pH and the buffer were identical to those used for Fig. 2*A* at pH 6.0. Although the gross features of the spectral changes at pH 8.5 were quite similar to those at pH 6.0, the absorption at 418 nm was almost unchanged during the entire reaction period (Fig. 2*b*). This result indicates that compound I scarcely accumulates at pH 8.5.

Detection of a New Spectral Species in the Reaction at pH 8.5—To uncover the difference in the reactions at pH 6.0 and 8.5, we analyzed the above spectral data by SVD. In general, SVD calculations transform an absorption data matrix (*i.e.* a set of time-resolved absorption spectra) into a product of three matrices, **U**, **S**, and $\mathbf{V}^t$, where the *i*th column of the matrix **U** is termed *i*th basis spectrum (44). Among the basis spectra, only a few columns from 1st to *n*th of the matrix **U** carry information about absorption spectra of the chemical species. Each of these basis spectra, which are called the significant basis spectra, can be expressed as an appropriate linear combination of the absorption spectra of the chemical species involved in the reaction (11, 42, 45–48). The total number, *n*, of the significant basis spectra corresponds to the minimal number of the chemical species that contributes to the absorption data matrix (11, 42, 45–48). Other basis spectra (>*n*) consist of optical noises and have no significant spectral features (11, 42, 45–48).

SVD calculations for the present data found three significant basis spectra for the reactions at pH 6.0 and 8.5. In Fig. 3, the first, second, and third basis spectra thus obtained at pH 6.0 are shown in *A–C*, whereas those at pH 8.5 are in *D–F*, respectively (*solid lines*). The presence of three significant basis spectra at both pH 6.0 and 8.5 indicates that the reaction involves at least three spectral species. We have assigned these to metMb, ferryl Mb, and another state of Mb, which is characterized below. The results at pH 6.0 are more easily interpreted because compound I can be detected due to its distinctive absorption changes (11). On the other hand, at pH 8.5 it is less clear that either compound I or any other well known species contributes to the absorption changes. We therefore simulated the above basis spectra in terms of linear combinations of optical absorption spectra of metMb, ferryl Mb, and compound I that were obtained independently.

The standard absorption spectra of metMb (*thin solid line*), ferryl Mb (*broken line*), and compound I (*thick solid line*) in Fig. 3*G* are used for the analyses. Among them, the spectrum of compound I is that reported for H64A mutant of sperm whale Mb by Matsui *et al.* (19).[2] According to Matsui *et al.*, compound

[2] Numerical data of the absorption spectrum of the mutant compound I was kindly provided by Drs. Toshitaka Matsui, Shinichi Ozaki, and Yoshihito Watanabe (19).

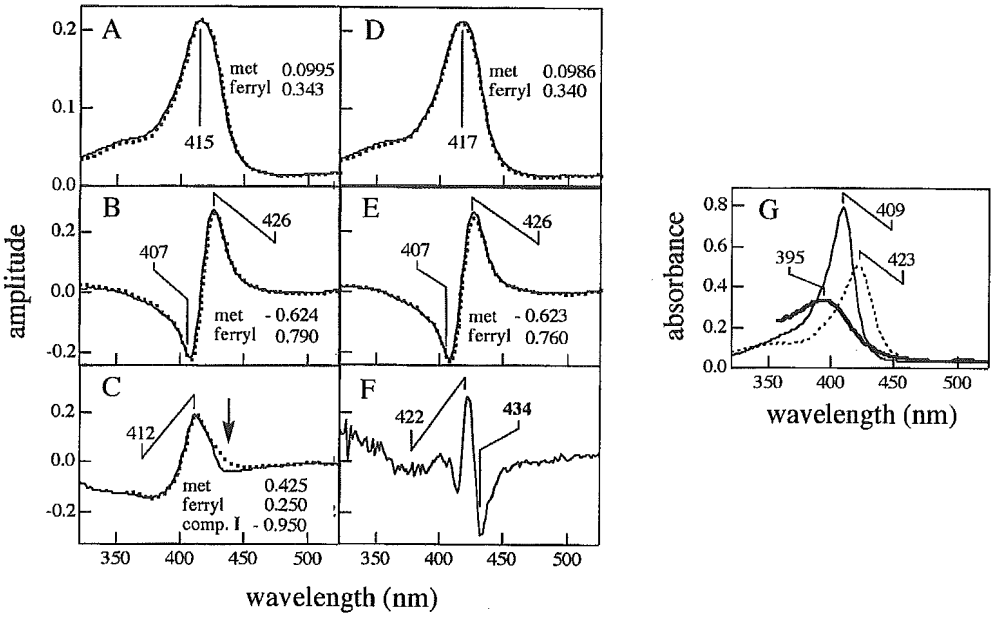

FIG. 3. **The significant basis spectra for the absorption changes in the reaction of sperm whale metMb with H_2O_2 at pH 6.0 (*A–C*) and 8.5 (*D–F*).** The first (*A* and *D*), second (*B* and *E*), and third (*C* and *F*) basis spectra are shown (*solid line*). The standard absorption spectra of metMb (*thin solid line*), ferryl Mb (*broken line*), and compound I (*thick solid line*) are indicated in *G*. The standard spectra of metMb and ferryl Mb were recorded by the stopped flow-rapid scan system; the former was recorded for metMb in absence of H_2O_2 at pH 6.0, whereas the latter is an average of absorption spectra at 400–500 ms of the reaction of metMb and H_2O_2 at pH 6.0. The standard spectrum of compound I was recorded for the H64A mutant of Mb (19).[2] All the basis spectra except for *F* could be reproduced by combining the standard absorption spectra of metMb, ferryl Mb, and compound I in *G*. The resultant linear combination spectra are shown in *A–E* (*broken lines*) with their linear combination factors. All the basis spectra in *A–F* were calculated from the sets of time-resolved absorption spectra represented in Fig. 2.

I was detectable as an almost pure product when *m*-chloroperoxybenzoic acid was added to ferric H64A Mb (19). It is also possible to obtain the absorption spectrum of compound I for the reaction of native Mb with H_2O_2 using a D_2O buffer system; however, contributions of metMb and ferryl Mb to the observed spectrum of compound I cannot be removed completely (11). As the standard absorption spectrum of metMb, a spectrum at pH 6.0 was utilized to analyze the basis spectra at both pH 6.0 and 8.5. Although the absorption spectrum of metMb is known to depend on pH and shows an acid-alkaline transition of the coordination state of the heme ($pK_a \sim 9$) (50), the spectrum was essentially unchanged in the pH range examined in our experiments (see spectra of metMb in Fig. 2, *A* and *B*). Although we observed gradual degradation of ferryl Mb into colorless product(s) of the heme under the current experimental conditions (data not shown), the degradation was much slower than the time period (<1 s) of our observations. We therefore obtained the standard spectrum of ferryl Mb (Fig. 3*G*, *broken line*) by averaging the time-resolved spectra from 400 to 500 ms recorded for the reaction at pH 6.0. The calculated spectrum agrees well with reported spectra of ferryl Mb (12, 14).

By using these standard spectra, we found that the first and second basis spectra at pH 6.0 were well reproduced by combining the standard spectra of metMb and ferryl Mb (*broken lines* in Fig. 3, *A* and *B*). Linear combination factors used for reproducing the basis spectrum were indicated on each panel. For example, the reproduced spectrum in Fig. 3*A* is given by 0.0995 × metMb spectrum + 0.343 × ferryl Mb spectrum. On the other hand, the reproduction of the third basis spectrum (Fig. 3*C*) required the standard absorption spectrum of compound I in addition to the spectra of metMb and ferryl Mb. The calculated spectrum (Fig. 3*C*, *broken line*) agrees well with the third basis spectrum (*solid line*) except for a slight deviation near 430 nm indicated by an arrow. The deviation will be discussed later.

The first and second basis spectra for the reaction at pH 8.5 are essentially the same as the corresponding spectra at pH 6.0 and were also well reproduced by combining the spectra of metMb and ferryl Mb (Fig. 3, *D* and *E*). On the other hand, the third basis spectrum at pH 8.5 (Fig. 3*F*) displays sharp negative and positive peaks at 434 and 422 nm, respectively, which are distinct from the third basis spectrum at pH 6.0. Among the standard absorption spectra in Fig. 3*G*, the ferryl Mb spectrum exhibits the Soret peak at 423 nm. Thus, the presence of the 422-nm peak in the third basis spectrum could be explained by the contribution of ferryl Mb. On the other hand, none of the standard spectra show a peak at the wavelength longer than 423 nm. Therefore, it is obviously impossible to reproduce the negative peak at 434 nm of the third basis spectrum at pH 8.5 by any combinations of the standard absorption spectra.

Because more than one chemical species contributes to each of the significant basis spectra, the negative peak position at 434 nm of the third basis spectrum (Fig. 3*F*) does not necessarily mean that the unidentified species exhibits an absorption peak at exactly 434 nm. The presence of the negative peak at 434 nm, which is red-shifted from the Soret absorption peak of ferryl Mb at 423 nm, rather indicates that the species exhibits a Soret band at a wavelength longer than 423 nm. This spectral characteristic is not typical of the ferric high spin species of heme proteins, which usually exhibits the Soret bands at 405–410 nm; it is more typical of the ferric low spin species (50). This finding indicates that an unidentified spectral species, which is distinct from compound I but is similar to ferric low spin compounds, temporarily accumulates in the reaction of metMb with H_2O_2 at pH 8.5.

The presence of the above unidentified species was not specific to the buffer system we employed. When the reaction was carried out in potassium phosphate buffer at pH 8.0, the shapes of the third basis spectrum was essentially unchanged (see below).

Time Profile of the Concentration of the New Spectral Species—According to the principle of SVD, *i*th row of the matrix $\mathbf{V}^t$ represents time progression of *i*th column of the matrix $\mathbf{U}$ (*i.e.* *i*th basis spectrum), and it can be expressed as an appropriate

linear combination of the actual time profiles of concentrations of the chemical species in the reaction (11, 42, 45–48). Thus, least squares analyses on $\mathbf{V}^t$ rows enable us to compute concentration changes of chemical species, if appropriate equations for the concentration changes are given (11, 42, 45–48). In the present study, however, this method did not work well; the computed value of the decay constant of the new intermediate at pH 8.5, which corresponds to k_2 in Reaction 1, was accompanied by a large error. Because the accumulated amount of the intermediate was very small, the signal-to-noise ratio of the third $\mathbf{V}^t$ row, which mostly carries information about the intermediate, was poor. The reaction was approximately a single exponential process, and only one apparent rate constant, which corresponds to k_1, was determined to be 2.4×10^{-1} s^{-1} at 50 mM H_2O_2. However, we could comprehend a rough trend of the concentration changes of the intermediate when we investigated singular values of the reaction.

In general, the ith singular value (*i.e.* ith diagonal elements of the matrix **S**) is a measure for contribution of ith basis spectrum to the absorption data matrix (45–48). Therefore, if extinction coefficients of a chemical species, which is represented by the ith basis spectrum, are not largely different from those of other chemical species in the reaction, the relative magnitude of ith singular value roughly corresponds to relative total concentration of that chemical species. For the reaction of metMb and H_2O_2 at pH 8.5, singular values of the first, second, and third basis spectra were 1.8×10^1, 2.6×10^0, and 1.0×10^{-2}, respectively. Among them, the first two represent both metMb and ferryl Mb; the first and second basis spectra are linear combinations of met and ferryl spectra (see Fig. 3, *D* and *E*). Considering the weights (*i.e.* absolute values of the linear combination factors) of the met spectrum (~0.1 and ~0.6 in the first and second basis spectra), the total contribution of the met spectrum to the absorption data matrix was determined to be $0.1(1.8 \times 10^1) + 0.6(2.6 \times 10^0) \approx 4 \times 10^0$. On the other hand, the intermediate is represented by the third basis spectrum (Fig. 3*F*) giving the third singular value (1.0×10^{-2}), and its weight in the third basis spectrum is at most 1. Based on these values, we determined that the total concentration of the intermediate was more than 2 orders of magnitude smaller than that of metMb. Thus, k_1/k_2 is less than 1×10^{-2} (see Equation 3). Based on this, together with the experimental value of k_1, we estimated the maximum accumulation time, t_{max}, of the intermediate to be <2 ms according to Equation 4.

On the other hand, when $k_1 \ll k_2$, Equation 2 can be reduced to Equation 5,

$$[I] = [R]_0 \frac{k_1}{k_2} \exp(-k_1 t) \qquad \text{(Eq. 5)}$$

Equation 5 indicates that concentration of intermediate species in such cases decreases at a rate (k_1) the same as decay rate of reactant. Accordingly, we determined that the concentration of the unidentified intermediate of Mb reached a maximum value within a very short time (<2 ms), which is shorter than the dead time (6 ms) of the stopped flow experiments, and decreased with decreasing the concentration of metMb. Based on these estimations, we planned rapid-freezing EPR experiments to identify the intermediate (see below).

Identification of the New Spectral Species by Rapid Freezing-EPR—To identify the new spectral species found at pH 8.5, a series of EPR experiments was carried out with the aid of the rapid freezing technique. The reaction was initiated by mixing 1 mM metMb and 200 mM H_2O_2 in a 1:1 ratio at pH 8.5 or pH 6.0; the concentrations of metMb and H_2O_2 (500 mM and 100 mM after the mixing) were larger by factors of 100 and 2, respectively, than those in the stopped flow-rapid scan experiments. The condition of the concentrations ($[H_2O_2] \gg$ [metMb]) allows the reaction be pseudo first-order with respect to H_2O_2; thus, the reaction is expected to proceed at a rate twice that in the stopped flow-rapid scan experiments. Since t_{max} of the intermediate is expected to be very small, we quenched the reaction within a short time (≤3 ms), which was comparable to the dead time of the stopped flow experiments.

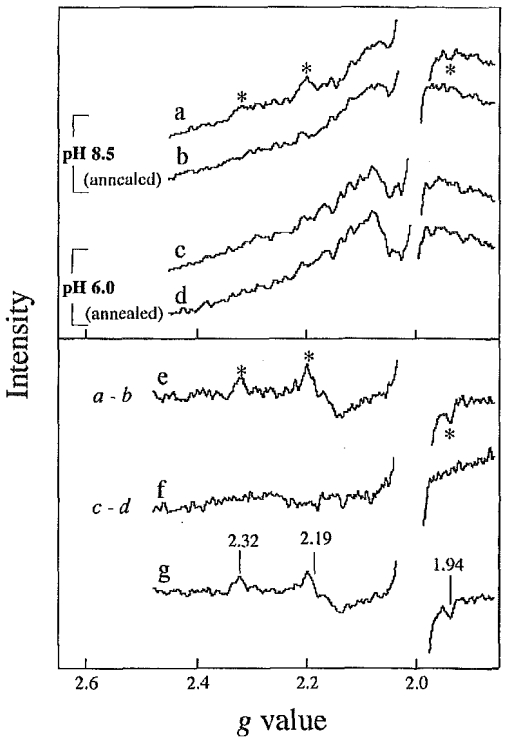

FIG. 4. **EPR spectra of the reaction mixtures of sperm whale metMb and H_2O_2 obtained by the rapid freezing techniques.** *Upper panel*, the reaction of metMb with H_2O_2 was started by mixing 1 mM metMb and 200 mM H_2O_2 solutions with a 1:1 ratio at room temperature and at pH 8.5 (*a* and *b*) or 6.0 (*c* and *d*). The reaction was then quenched within 3 ms by freezing the reaction mixture at 77 K. X-band EPR spectra of the frozen samples were measured at 15 K. Spectra *b* and *d* were measured for the same samples that gave spectra *a* and *c*, respectively, after annealing the samples at 220 K for 150 s. Buffer systems were the same as those indicated in Fig. 2. *Lower panel*, the difference EPR spectra calculated by subtracting the EPR spectra after the annealing from those before the annealing at each pH. Trace *e* and *f* represent the difference between traces *a* and *b* and between *c* and *d*, respectively. Spectrum *g* is an average of the two difference spectra including trace *e* obtained from the two independent experiments conducted at pH 8.5.

Fig. 4 illustrates the EPR spectra of the quenched samples measured at 15 K. Although the sample prepared at pH 8.5 (spectrum *a*) showed several peaks (*asterisks*), the signal-to-noise ratio was rather poor. We therefore raised the temperature of the sample to 220 K for 150 s (annealing), expecting that the intermediate species, if any, would decompose without drastic alterations of the sample conditions. After the annealing, the sample was cooled to 15 K, and the EPR spectrum was recorded again. The spectrum thus obtained (spectrum *b*) indicates that several signals presented before the annealing disappeared or were weakened. The changes are more clearly shown in the difference spectrum (spectrum *e*: spectrum *a* *minus* spectrum *b*), which clearly indicates the presence of the signals marked with *asterisks* in spectrum *a*. On the other hand, the EPR spectra collected before and after the annealing (spectra *c* and *d*, respectively) at pH 6.0 were essentially the same, and their difference spectrum (spectrum *f*) did not give any of the notable EPR signals observed at pH 8.5.

In order to improve the signal-to-noise ratio, we repeated the

same experiments at pH 8.5, and we averaged the difference spectra. The averaged spectrum (spectrum *g*) gave us a set of *g* values at 2.32, 2.19, and 1.94. Because the *g* values for ferric hydroperoxy hemes (Fe(III)–[O–O–H]$^-$) were reported at 2.25–37, 2.16–9, and 1.91–6 (34–39, 51), the current data indicate the formation of a hydroperoxy compound in the reaction of metMb with H_2O_2 at pH 8.5. It should be noted that the *g* values of the ferric hydroperoxy hemes are unique and distinct from those of other ligand complexes of ferric and ferrous iron porphyrins, and therefore, they serve as an unmistakable signature of the Fe(III)–[O—O–H]$^-$ structure (34–39, 51).

By using rapid freezing-EPR techniques, Brittain *et al.* (51) detected EPR signals of hydroperoxy species in reactions of distal histidine mutants (H64V and H64Q) of sperm whale metMb with H_2O_2 at pH 7.5, although corresponding EPR signals were not detected for wild type metMb under their experimental conditions. In our EPR experiments, the hydroperoxy signals were detected together with an EPR signal giving positive and negative peaks around $g \sim 2$, which was assigned to the amino acid radical of ferryl Mb formed within the quenching dead time. We found that the hydroperoxy signals were 2 orders of magnitude weaker than the radical signal (data not shown). On the other hand, in the experiments by Brittain *et al.* (51) for H64Q mutant, the observed EPR intensities of hydroperoxy signals were comparable with that of the amino acid radical signal of ferryl Mb at a wide range (9–44 ms) of quenching dead time (see Fig. 4*A* of Ref. 51) that covered t_{max} of the hydroperoxy compound (20 ms) under their conditions. Therefore, we estimate that the accumulated amount of the hydroperoxy intermediate relative to ferryl Mb was at least 2 orders of magnitude smaller in native Mb than in the mutant. This further means that the concentration of the hydroperoxy intermediate in our EPR experiments was at least 2 orders of magnitude smaller than the total concentration of Mb. By careful examinations of the pH effects on the reaction kinetics and the use of a higher concentration of Mb in the EPR experiments, we successfully detected the hydroperoxy compound in native metMb.

We assigned the new spectral species of Mb detected by the SVD analyses to the hydroperoxy compound observed by the EPR experiments on the following bases. 1) The SVD analysis indicated that the concentration of the new spectral species, which was the sole detectable intermediate at pH 8.5 and distinct from heme degradation products, reaches the maximum value within a very short time (<2 ms) and decreases relatively slowly as the reaction proceeds. Therefore, the hydroperoxy compound detected for the samples quenched within 3 ms should be assigned to the spectral species. Although we did not carry out rapid freezing-EPR experiments at a freezing dead time longer than 3 ms, the annealing experiments are reasonable alternatives to such experiments; when the reaction proceeded upon the annealing, the hydroperoxy signals quenched at 3 ms indeed disappeared. 2) The pH dependence of the new spectral species and the hydroperoxy EPR signals agree with each other; they were detected at pH 8.5 but were not detected at pH 6.0. 3) The low spin type Soret band ($\lambda_{max} \geq$ 423 nm) of the spectral species is consistent with the assignment, because the hydroperoxy hemes are ferric low spin species (34–39, 51).

Although the estimations were rough, the agreement between the populations of the new spectral species and the hydroperoxy species in the EPR experiments may further support the assignment; they both were estimated to be less than 1% of total Mb. Accordingly, we conclude that the unidentified intermediate species in the reaction of metMb with H_2O_2 at pH 8.5 is the hydroperoxy compound of Mb.

Effects of pH on the Kinetics of the Reaction—The present results indicate that the reaction of metMb with H_2O_2 is pH-dependent. Acidic conditions are favorable for the accumulation of compound I, and alkaline conditions favor accumulation of the hydroperoxy compound. Because the pH-dependent changes of the reaction strongly suggest the participation of the distal amino acid residues, we further analyzed the pH dependence based on extensive pH titration experiments. We measured and analyzed absorption changes of the reaction in a pH range from 6.25 to 8.0. The SVD analyses indicated that the number of the significant basis spectra was 3 at every pH condition and that the first and second basis spectra did not depend on pH (data not shown). The changes in the third basis spectrum at pH 6.25–8.0 were illustrated in Fig. 5*A*, where directions of the spectral changes upon rising pH were indicated by *arrows*. The spectral difference amplitudes between the positive peak at 422 nm and the negative peak at 434 nm are plotted *versus* pH in Fig. 5*E* (*closed circles*). The plot for sperm whale metMb agrees well with a theoretical titration curve (*thick solid line*) using a single pK_a value of 7.27. This result indicates that the protonation state of a certain chemical group regulates the conversion of the third basis spectrum and gives an apparent pK_a (hereafter termed as pK_a^{app}) for the transition of the kinetics. The most plausible origin of the pK_a^{app} value at around pH 7 is the distal histidine (His-64) located in the close vicinity of the heme, because all other amino acid residues facing the distal heme pocket of Mb (Ile-28, Leu-29, Phe-43, and Val-68) (27) are not ionizable.

As described earlier, the third basis spectrum at pH 6.0 could not be fully reproduced by any linear combinations of the standard spectra of metMb, ferryl Mb, and compound I due to the negative shoulder near 430 nm (see Fig. 3*C*). The titration plot (Fig. 5*E*, *closed circles*) indicates that the transition to the acid state is not complete at pH 6.0, and a small amount of the hydroperoxy compound is formed at pH 6.0. The negative shoulder in the spectrum of Fig. 3*C* may therefore be attributable to the hydroperoxy compound. The present reaction obviously involves four chemical species, *i.e.* metMb, the hydroperoxy compound, compound I, and ferryl Mb, at around pH 7, but only three significant basis spectra were obtained. This is possibly because the accumulated amounts of compound I and the hydroperoxy compound were very small. The absorption spectra of the hydroperoxy compound and compound I were combined and appeared on each of the third basis spectrum in Fig. 5*A*, and the relative population of these two compounds at the given pH reflected the shapes of each third basis spectrum.

The changes in the third basis spectrum observed for sperm whale Mb were reproducible in horse heart (Fig. 5*B*) and human (Fig. 5*C*) Mbs. These results indicate that the accumulation observed here of compound I under acidic and the hydroperoxy compound under alkaline conditions are commonly encountered for reactions between H_2O_2 and Mb species. As shown in Fig. 5*E*, the pK_a^{app} values for the different species of metMb were quite similar. They were 7.18 and 7.00 for horse heart (Fig. 5*E*, *open circles* and *thin solid line*) and human (*closed triangles* and *thick broken line*) Mbs, respectively. Interestingly, the pK_a^{app} of Mbs (sperm whale, 7.27 > horse heart, 7.18 > human, 7.00) roughly parallels pK_a of the acid-alkaline transition, which reflects ability of the distal histidine to abstract a proton from a ligand water, at the Met state of these Mbs. Reported values of pK_a of the acid-alkaline transition, pK_a^{AB}, are as follows: sperm whale, 8.99 > horse heart, 8.93 > human, 8.72 (41, 50). In order to examine further this parallel relationship, we carried out experiments with a mutant of human Mb (T67N), which shows a pK_a^{AB} value (8.49) lower than

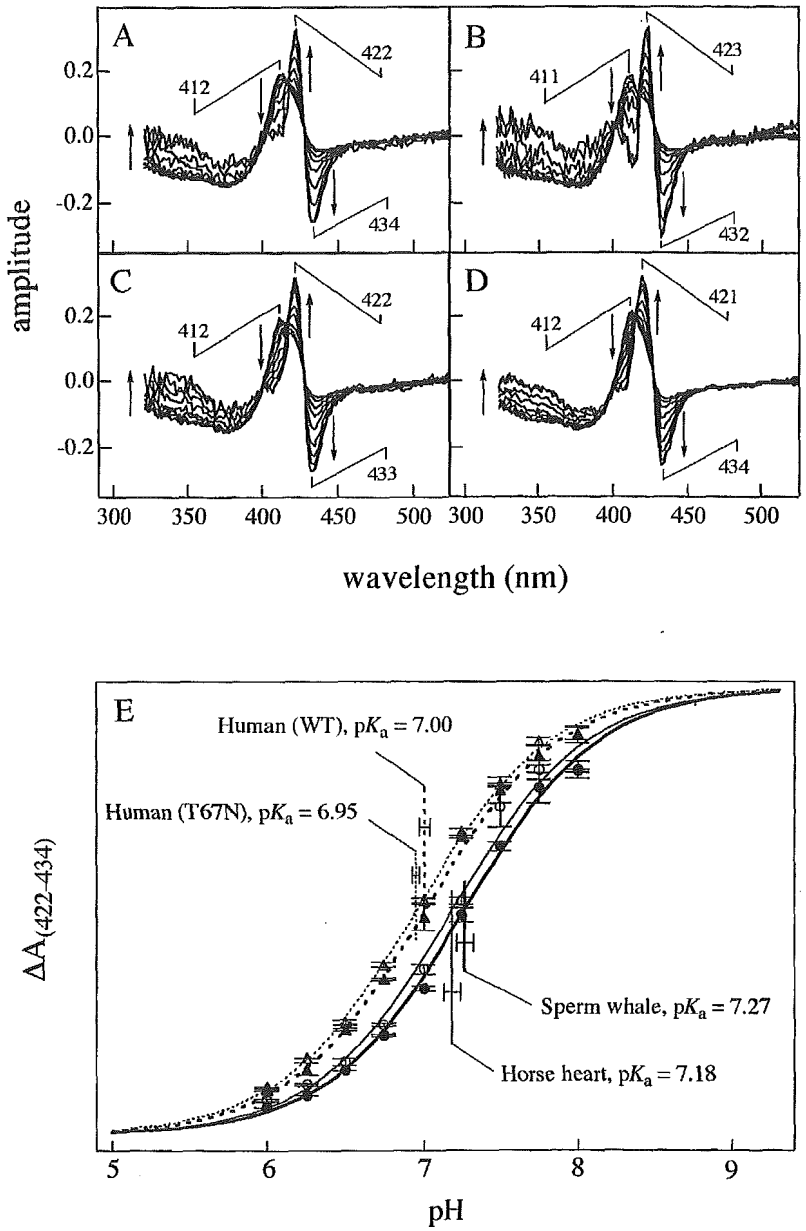

FIG. 5. **Effects of pH on the accumulation kinetics of the hydroperoxy compound represented by changes in the SVD third basis spectrum.** *A–D*, the third basis spectrum was obtained for the reactions of sperm whale (*A*), horse heart (*B*), wild type human (*C*), and human T67N mutant (*D*) metMbs with H_2O_2 at the pH range from 6.25 to 8.0. *Arrows* in each panel indicate directions of spectral changes upon rising pH. All the data in *A–D* were obtained for 5 μM metMbs and 50 mM H_2O_2 at 25 °C. Buffer was 200 mM potassium phosphate. *E*, the difference spectral amplitudes at 422 and 434 nm in the third basis spectra of sperm whale (*closed circle*), horse heart (*open circle*), wild type human (*closed triangle*), and human T67N mutant (*open triangle*) Mbs were plotted against pH. The vertical scale of each plot was normalized. The data represent the mean ± S.D. of three experiments except for those of the wild type human Mb at pH 6.75 and 7.25, which are expressed as the mean and the deviation of two experiments. The theoretical pH titration curves (sperm whale, *thick solid*; horse heart, *thin solid*; wild type human, *thick broken*; human T67N, *thin broken*) were calculated by assuming an ionization of one chemical group. *Vertical lines* show pK_a values (mean ± S.D.) of the theoretical titration curves.

that of wild type human metMb (41). The mutant also showed significant changes in the SVD third basis spectrum (Fig. 5*D*), and the pK_a^{app} of the spectral changes was indeed shifted to a lower value (6.95) from that of the wild type protein (Fig. 5*E*, *open triangles* and *thin broken line*). This confirms the parallel relationship. Meanings of this relationship are discussed later.

Association Rate between metMb and H_2O_2—The apparent decay of metMb could be approximated to a single pseudo first-order exponential process. The rate of the process corresponds to association rate between metMb and H_2O_2. The estimated association rate constant for sperm whale metMb at pH 7.0 was 4.8×10^2 (M^{-1} s^{-1}), which is in reasonable agreement with the reported values (14, 52). The association rate constant was decreased slightly under both of the acidic and alkaline conditions (data not shown), but no obvious pK_a value related to pK_a^{app} was observed. Similar results were also obtained for other Mbs examined here. Therefore, the chemical step(s) that are subjected to the pH effect and give pK_a^{app} are not involved in the association processes of H_2O_2 to the ferric heme of metMb.

DISCUSSION

In this study, we investigated the reaction between metMb and H_2O_2, and we obtained evidence for the formation of the hydroperoxy compound in the reaction. It was also demonstrated that the distal histidine plays key roles in accumulation of the hydroperoxy compound. These results give insights into the mechanism of the O–O bond activation in metMb and in heme peroxidases.

Reaction Mechanisms—The entire reaction between H_2O_2 and ferric heme proteins consists of the association of H_2O_2 to the ferric heme and the subsequent chemical steps including the cleavage of the O–O bond. The association process involves a diffusion of H_2O_2 into the heme pocket and the coordination of H_2O_2 to the ferric heme, which leads to the formation of the ferric heme-H_2O_2 complex (Fig. 1, $a \rightarrow b$) (20–22, 25). For the reaction between metMb and H_2O_2, the pH dependence of the association process does not correlate with the apparent pK_a (pK_a^{app}) of the accumulation kinetics for the hydroperoxy compound. Therefore, the step(s) controlled by the distal histidine most likely occur after the formation of the Mb-H_2O_2 complex.

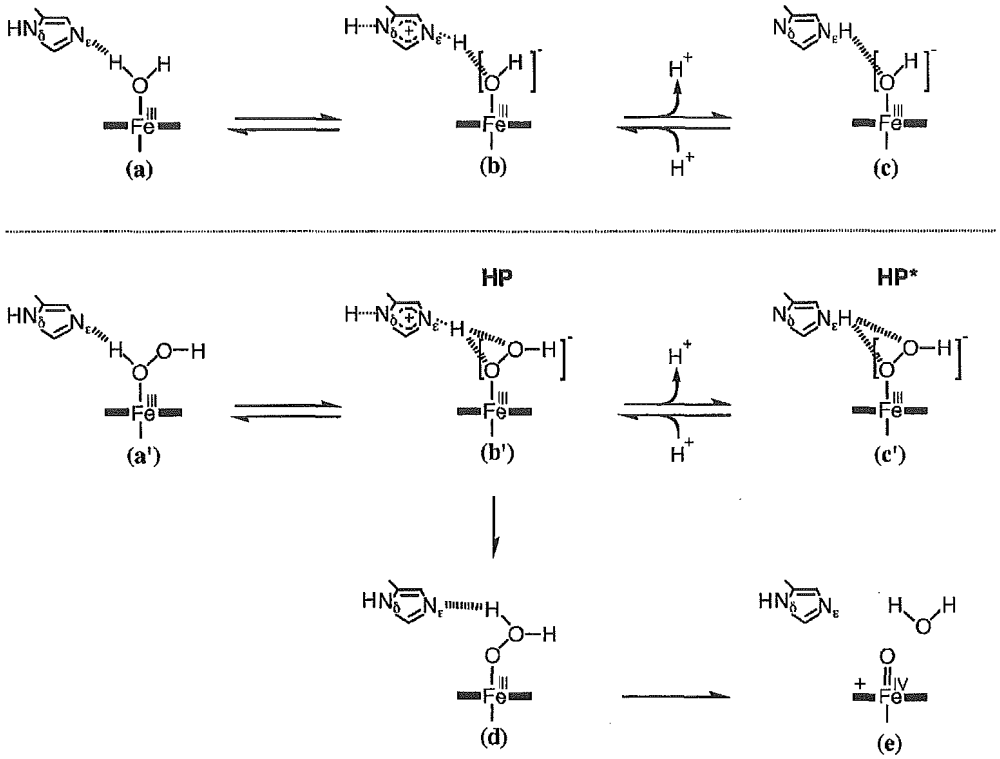

FIG. 6. **The acid-alkaline transition of metMb (*a–c, upper*) and the proposed mechanisms for the reaction of metMb with H_2O_2 regulated by the protonation status of the distal histidine (*a'–c', d,* and *e, lower*).** The equilibrium schemes of the acid-alkaline transition (*a–c*) are drawn on the basis of Ref. 50. *Thick broken lines* in both *upper* and *lower* schemes represent hydrogen bonds, and *thin broken lines* in *b* and *b'* represent lengthened covalent bonds. The species *b'* and *c'* are termed also as *HP* and *HP**, respectively, as described in the text.

Thus, the conversion from the Mb-H_2O_2 complex to the hydroperoxy compound and/or the decomposition of the hydroperoxy compound are affected by the distal histidine. This conclusion is consistent with the mechanism proposed by Poulos and Kraut (26) in which the distal histidine catalyzes both of the formation and decomposition of the hydroperoxy intermediate in peroxidases.

In order to discuss further details on possible mechanisms of the reaction of metMb with H_2O_2, we first consider the origin of the pK_a of the acid-alkaline transition, pK_a^{AB}, to which pK_a^{app} showed a parallel relationship. In the *upper panel* of Fig. 6 (*a–c*), the schemes for the acid-alkaline transition are illustrated. Under acidic conditions, Nϵ of the distal histidine forms a hydrogen bond with a proton of the ligand water of the heme, whereas Nδ is protonated (Fig. 6*a*) (50). Under alkaline conditions, Nδ releases its proton, and Nϵ accepts a proton from the water, converting the ligand water to hydroxide anion (Fig. 6*c*) (50). The transient state between the acid and alkaline forms can be drawn as Fig. 6*b*; one proton is to be released from Nδ and the other proton is approaching from the ligand water to the Nϵ nitrogen, allowing the distal histidine to be an imidazolium-like structure.

By analogy to the above schemes, we can reasonably draw schemes of two equilibria (Fig. 6, *a'* ↔ b' ↔ *c'*), which are expected to occur when an H_2O_2 molecule replaces the ligand water of metMb. It should be noted that the left equilibrium (*a'* ↔ *b'*) has a formula essentially the same as that involved in the Poulos and Kraut mechanism for the peroxidase reaction (Fig. 1, *b* ↔ *c*). On the other hand, the other equilibrium (Fig. 6, *b'* ↔ *c'*), in which the protonation state at the Nδ nitrogen of the distal histidine is changed, is not involved in the Poulos and Kraut mechanism. In the Poulos and Kraut mechanism, the imidazolium form of the distal histidine donates its Nϵ proton to the terminal oxygen of the hydroperoxy group (acid catalysis) and assists the heterolytic O–O bond cleavage. This reaction path was also depicted in Fig. 6 (*b'* → *d* → *e*). Although it may be possible that an O–O bond cleavage reaction proceeds also from the hydroperoxy state of Fig. 6*c'* (termed as HP* state, hereafter), this state should be more stable against the O–O bond cleavage than the other hydroperoxy state (Fig. 6*b'*, termed as HP state), because imidazole (in HP*) is a poor acid as compared with imidazolium (in HP). Thus, O–O bond cleavage path from the HP* state was excluded from the entire schemes of Fig. 6. Then the amount of the HP* state transiently accumulated in the reaction between metMb and H_2O_2 under given pH should be determined essentially by pK_a of the equilibrium between the HP* and HP states.

Because the ferric heme and the distal histidine concertedly facilitate the ionization of the ligand water, pK_a^{AB} is significantly down-shifted to ~9 from the intrinsic pK_a value of water at ~16 (50). In addition, pK_a^{AB} varies slightly with different species of Mb and depends on the slight conformational variations of the distal histidine and the chemical environment of the heme pockets. Thus, sperm whale, horse heart, human, and human T67N mutant Mbs exhibit different pK_a^{AB} values (41, 50). Similarly, it is expected that the pK_a value of the equilibrium between the HP and HP* states is lower than the intrinsic pK_a of H_2O_2 (~12), which is remarkably lower than that of water (~16). Therefore, the pK_a value is also expected to be lower than pK_a^{AB} and to show a variation that parallels pK_a^{AB}. When the pH is below this pK_a value, heterolysis and the formation of compound I is favored (Fig. 6, *b'* → *d* → *e*), whereas above the pK_a value, stabilization of the HP* state is favored.

The above mechanism for the reaction of metMb with H_2O_2 was proposed on the basis of the established knowledge on the acid-alkaline transition of Mb, the acid characteristics of imidazole and imidazolium, and the chemical characteristics of H_2O and H_2O_2. It should be emphasized that the present observations are fully consistent with the mechanism thus proposed; the stable hydroperoxy intermediate, that is HP*, was detect-

able only under alkaline conditions; the pK_a value (~7) with respect to the accumulation of the intermediate, pK_a^{app}, was significantly lower than pK_a^{AB} (~9); pK_a^{app} parallels pK_a^{AB}.

Implication for the Heme Peroxidase Reactions—We have proposed a detailed molecular mechanism for the reaction of metMb with H_2O_2. The mechanism shares the elementary chemical steps with the Poulos and Kraut mechanism, but the deprotonation equilibrium at the Nε nitrogen is newly added. We further suggest that the equilibrium is biased to the protonated form in heme peroxidases to facilitate the H_2O_2 activation. Our suggestion is based on the knowledge on amino acid residues that form the heme pockets of the peroxidases as follows.

X-ray crystallographic studies have indicated that the Cχ carbonyl of a conserved asparagine in heme peroxidases (Asn-70 of HRP, Asn-82 of *Cc*P, or Asn-84 of lignin peroxidase, LiP), which is not found in Mb, forms a hydrogen bond with Nδ of the distal histidine (53–55). This hydrogen bond is expected to restrain the proton release from the Nδ nitrogen. Such a function of the conserved asparagine (distal asparagine) has been clearly demonstrated in the ferric cyanide complexes of HRP (56), *Cc*P (57), and LiP (58) by proton NMR techniques. When cyanide binds to the ferric heme of these peroxidases, the proton of HCN is transferred to the Nε nitrogen of the distal histidine, whereas Nδ remains protonated, allowing the histidine to be in the imidazolium form (56–58). On the other hand, in the corresponding cyanide complex of sperm whale metMb, the distal histidine can accept the proton from HCN at the Nε nitrogen and releases the Nδ proton to remain in the imidazole form (59). These observations strongly suggest that the Nδ nitrogen of the distal histidine in peroxidases is also resistant to deprotonation during the H_2O_2 catalysis. The formation of a stable hydroperoxy species corresponding to the HP* state (Fig. 6*c*′) should be suppressed in the peroxidases, because the formation is coupled with the deprotonation at the Nδ nitrogen (Fig. 6, $b' \rightarrow c'$). Thus, the reaction of the peroxidases with H_2O_2 should proceed according to the Poulos and Kraut mechanism without accumulating the stable hydroperoxy state. This proposal is consistent with the observations that the detection of the hydroperoxy species was difficult for the reactions of the peroxidases with H_2O_2 but was successful for the corresponding reaction of metMb as demonstrated in this study.

Nagano *et al.* (60) prepared the distal asparagine mutants (N70V and N70D) of HRP, and showed that the rate of the compound I formation by H_2O_2 was decreased by an order of magnitude in the mutants. One of the mutants, N70D, was subjected to detailed proton NMR experiments in the ferric cyanide state (61). The NMR experiments indicated that the distal histidine of the cyanide complex of the mutant possesses the Nε and Nδ protons, but the Nδ proton signal showed significant broadening, which was not found for the wild type cyanide complex. This was attributed to a rapid exchange of the Nδ proton with protons of bulk water (61). These results indicate that the distal asparagine of HRP indeed hinders the release of the Nδ proton effectively. Although it was not examined whether the hydroperoxy compound was detectable in the mutants, their decreased rates of compound I formation are consistent with the suggestion that the distal asparagine suppresses the formation of the HP* state and accelerates the compound I formation.

Acknowledgments—We thank Dr. Takeshi Uchida (Institute for Molecular Science, Japan) for preparing the samples of wild type and T67N mutant of human Mb. We are also grateful to Dr. Takashi Yonetani (University of Pennsylvania, Philadelphia) for helpful discussions and for critically reviewing the manuscript.

REFERENCES

1. Schonbaum, G. R., and Chance, B. (1976) in *The Enzymes* (Boyer, P. D., ed) Vol. 13, pp. 363–408, Academic Press, New York
2. Yonetani, T. (1976) in *The Enzymes* (Boyer, P. D., ed) Vol. 13, pp. 345–361, Academic Press, New York
3. Dunford, H. B., and Stillman, J. S. (1976) *Coord. Chem. Rev.* **19,** 187–251
4. Hewson, W. D., and Hager, L. P. (1979) in *The Porphyrins* (Dolphin, D., ed) Vol. 7, pp. 295–332, Academic Press, New York
5. Agner, K. (1941) *Acta Chem. Scand.* **2,** Suppl. 8, 1–62
6. Harrison, J. E., and Schultz, J. (1976) *J. Biol. Chem.* **251,** 1371–1374
7. Blée, E., and Schuber, F. (1990) *J. Biol. Chem.* **265,** 12887–12894
8. Marcinkeviciene, J. A., Magliozzo, R. S., and Blanchard, J. S. (1995) *J. Biol. Chem.* **270,** 22290–22295
9. Nagy, J. M., Cass, A. E. G., and Brown, K. A. (1997) *J. Biol. Chem.* **272,** 31265–31271
10. Johnsson, K., Froland, W. A., and Schultz, P. G. (1997) *J. Biol. Chem.* **272,** 2834–2840
11. Egawa, T., Shimada, H., and Ishimura, Y. (2000) *J. Biol. Chem.* **275,** 34858–34866
12. George, P., and Irvine, D. H. (1952) *Biochem. J.* **52,** 511–517
13. King, N. K., Looney, F. D., and Winfield, M. E. (1967) *Biochim. Biophys. Acta* **133,** 65–82
14. Yonetani, T., and Schleyer, H. (1967) *J. Biol. Chem.* **242,** 1974–1979
15. Ortiz de Montellano, P. R., and Catalano, C. E. (1985) *J. Biol. Chem.* **260,** 9265–9271
16. Grisham, M. B. (1985) *J. Free Radicals Biol. Med.* **1,** 227–232
17. Galaris, D., Sevanian, A., Cadenas, E., and Hochstein, P. (1990) *Arch. Biochem. Biophys.* **281,** 163–169
18. Adachi, S., Nagano, S., Ishimori, K., Watanabe, Y., Morishima, I., Egawa, T., and Kitagawa, T. (1993) *Biochemistry* **32,** 241–252
19. Matsui, T., Ozaki, S., and Watanabe, Y. (1997) *J. Biol. Chem.* **272,** 32735–32738
20. Woon, D. E., and Loew, G. H. (1998) *J. Phys. Chem. A* **102,** 10380–10384
21. Filizola, M., and Loew, G. H. (2000) *J. Am. Chem. Soc.* **122,** 18–25
22. Wirstam, M., Blomberg, M. R. A., and Siegbahn, P. E. M. (1999) *J. Am. Chem. Soc.* **121,** 10178–10185
23. Palamakumbura, A. H., Vitello, L. B., and Erman, J. E. (1999) *Biochemistry* **38,** 15653–15658
24. Palamakumbura, A. H., Foshay, M. C., Vitello, L. B., and Erman, J. E. (1999) *Biochemistry* **38,** 15647–15652
25. Rodríguez-López, J. N., Lowe, D. J., Hernández-Ruiz, J., Hiner, A. N. P., García-Cánovas, F., and Thorneley, R. N. F. (2001) *J. Am. Chem. Soc.* **123,** 11838–11847
26. Poulos, T. L., and Kraut, J. (1980) *J. Biol. Chem.* **255,** 8199–8205
27. Antonini, E., Brunori, M. (1971) in *Hemoglobin and Myoglobin in Their Reactions with Ligands* (Neuberger, A., and Tatum, E. L., eds) Vol. 21, pp. 55–97, North-Holland Publishing Co., Amsterdam
28. Erman, J. E., Vitello, L. B., Miller, M. A., and Kraut, J. (1992) *J. Am. Chem. Soc.* **114,** 6592–6593
29. Erman, J. E., Vitello, L. B., Miller, M. A., Shaw, A., Brown, K. A., and Kraut, J. (1993) *Biochemistry* **32,** 9798–9806
30. Newmyer, S. L., and Ortiz de Montellano, P. R. (1995) *J. Biol. Chem.* **270,** 19430–19438
31. Savenkova, M. I., Newmyer, S. L., and Ortiz de Montellano, P. R. (1996) *J. Biol. Chem.* **271,** 24598–24603
32. Baek, H. K., and Van Wart, H. E. (1989) *Biochemistry* **28,** 5714–5719
33. Ozaki, S., Inada, Y., and Watanabe, Y. (1998) *J. Am. Chem. Soc.* **120,** 8020–8025
34. Symons, M. C. R., and Peterson, R. L. (1978) *Biochim. Biophys. Acta* **535,** 241–246
35. Gasyna, Z. (1979) *FEBS Lett.* **106,** 213–218
36. Davydov, R. M., Yoshida, T., Ikeda-Saito, M., and Hoffman, B. M. (1999) *J. Am. Chem. Soc.* **121,** 10656–10657
37. Davydov, R., Macdonald, I. D. G., Makris, T. M., Sligar, S. G., and Hoffman, B. M. (1999) *J. Am. Chem. Soc.* **121,** 10654–10655
38. Denisov, I. G., Makris, T. M., and Sligar, S. G. (2002) *J. Biol. Chem.* **277,** 42706–42710
39. Tajima, K. (1989) *Inorg. Chim. Acta* **163,** 115–122
40. Tanaka, M., Matsuura, K., Yoshioka, S., Takahashi, S., Ishimori, K., Hori, H., and Morishima, I. (2003) *Biophys. J.* **84,** 1998–2004
41. Nagano, S. (1985) *Roles of the Active Site Residues in Catalytic Activities of Heme Enzymes*, Ph.D. thesis, Kyoto University, Kyoto, Japan
42. Egawa, T., Shimada, H., and Ishimura, Y. (1994) *Biochem. Biophys. Res. Commun.* **201,** 1464–1469
43. Tonomura, B., Nakatani, H., Ohnishi, M., Yamaguchi-Ito, J., and Hiromi, K. (1978) *Anal. Biochem.* **84,** 370–383
44. Golub, G. H., and Kahan, W. (1965) *SIAM J. Num. Anal.* **2,** 205–224
45. Hofrichter, J., Henry, E. R., Sommer, J. H., Deutsch, R., Ikeda-Saito, M., Yonetani, T., and Eaton, W. A. (1985) *Biochemistry* **24,** 2667–2679
46. Hug, S. J., Lewis, J. W., Einterz, C. M., Thorgeirsson, T. E., and Kliger, D. S. (1990) *Biochemistry* **29,** 1475–1485
47. Lambright, D. G., Balasubramanian, S., and Boxer, S. G. (1993) *Biochemistry* **32,** 10116–10124
48. Walda, K. N., Liu, X. Y., Sharma, V. S., and Magde, D. (1994) *Biochemistry* **33,** 2198–2209
49. Szabó, Z. G. (1969) in *Comprehensive Chemical Kinetics* (Bamford, C. H., and Tipper, C. F. H., eds) Vol. 2, pp. 1–31, Elsevier Science Publishing Co., Inc., New York
50. Antonini, E., and Brunori, M. (1971) in *Hemoglobin and Myoglobin in Their Reactions with Ligands* (Neuberger, A., and Tatum, E. L., eds) Vol. 21, pp. 40–54, North-Holland Publishing Co., Amsterdam
51. Brittain, T., Baker, A. R., Butler, C. S., Little, R. H., Lowe, D. J., Greenwood,

C., and Watmough, N. J. (1997) *Biochem. J.* **326,** 109–115
52. Matsui, T., Ozaki, S., Liong, E., Phillips, G. N., and Watanabe, Y. (1999) *J. Biol. Chem.* **274,** 2838–2844
53. Gajhede, M., Schuller, D. J., Henriksen, A., Smith, A. T., and Poulos, T. L. (1997) *Nat. Struct. Biol.* **4,** 1032–1038
54. Finzel, B. C., Poulos, T. L., and Kraut, J. (1984) *J. Biol. Chem.* **259,** 13027–13036
55. Poulos, T. L., Edwards, S. L., Wariishi, H., and Gold, M. H. (1993) *J. Biol. Chem.* **268,** 4429–4440
56. Thanabal, V., de Ropp, J. S., and La Mar, G. N. (1987) *J. Am. Chem. Soc.* **109,** 7516–7525
57. Satterlee, J. D., and Erman, J. E. (1991) *Biochemistry* **30,** 4398–4405
58. de Ropp, J. S., La Mar, G. N., Wariishi, H., and Gold, M. H. (1991) *J. Biol. Chem.* **266,** 15001–15008
59. Cutnell, J. D., La Mar, G. N., and Kong, S. B. (1981) *J. Am. Chem. Soc.* **103,** 3567–3572
60. Nagano, S., Tanaka, M., Ishimori, K., Watanabe, Y., and Morishima, I. (1996) *Biochemistry* **35,** 14251–14258
61. Tanaka, M., Nagano, S., Ishimori, K., and Morishima, I. (1997) *Biochemistry* **36,** 9791–9798

ANTIOXIDANTS & REDOX SIGNALING
Volume 5, Number 4, 2003

Forum Original Research Communication

Carbon Monoxide Stimulates mrp2-Dependent Excretion of Bilirubin-IXα into Bile in the Perfused Rat Liver

SHINJI NORIMIZU,[1] ATSUSHI KUDO,[2] MAYUMI KAJIMURA,[2] KAZUO ISHIKAWA,[2] HISASHI TANIAI,[2] TOKIO YAMAGUCHI,[2] KIMIHITO FUJII,[2] SHIGEKI ARII,[2] YUJI NIMURA,[1] and MAKOTO SUEMATSU[2]

ABSTRACT

Although carbon monoxide (CO) has been reported to protect against hepatobiliary dysfunction, mechanisms for its actions remain unknown. This study aimed to examine actions of physiologically relevant concentrations of CO on biliary excretion. The effects of transportal administration of CO on bile output and constituents were examined in perfused rat livers. In livers of fed rats, CO regulated bile output biphasically in a dose-dependent manner; transportal administration of CO at 4 μmol/L stimulated bile output by 10%. Under these circumstances, CO increased paracellular junctional permeability and consequently decreased biliary excretion of bile salts. Choleresis elicited by 4 μmol/L CO coincided with significant increases in biliary excretion of bilirubin-IXα and glutathione. The CO-induced choleresis occurred independently of cyclic GMP, coincided with elevated excretion of K^+ and HCO_3^-, and was abolished by tetraethylammonium, suggesting stimulatory effects of the gas on potassium channels. CO-mediated choleresis and increased excretion of organic anions appeared to be mediated by mrp2, because Eisai hyperbilirubinemia rats, which genetically lack the transporter, did not exhibit choleresis upon the CO administration. These results suggest that CO stimulates mrp2-dependent excretion of bilirubin-IXα through mechanisms involving potassium channels, serving as a cooperator standing behind the heme oxygenase reaction to facilitate hepatic heme detoxification. *Antioxid. Redox Signal.* 5, 449–456.

INTRODUCTION

LIVER is a major organ responsible for detoxification of biologically active mediators and xenobiotics and for biliary excretion of their metabolites. These two processes occur through distinct metabolic processes. The former involves enzymatic modification of the noxious substrates by oxygenases and conjugation that can increase hydrophilicity of the compounds, whereas the latter involves excretion of their reaction products by specific transporters expressed at the hepatocellular membrane (10). A variety of endogenous organic compounds, such as bilirubin and leukotrienes, undergo such detoxification processes. Bilirubin is produced as an end product of the heme detoxification via the reaction of heme oxygenase (HO) and biliverdin reductase and is conjugated by glucuronyl transferase (14, 22). This bile pigment possesses a potent antioxidant action that ameliorates acute inflammatory processes (5). On the other hand, leukotrienes are produced by 5-lipoxygenase-mediated oxygenation of arachidonic acid and undergo glutathione conjugation prior to their excretion into bile (10). The reduced form of glutathione (GSH), a potent antioxidant that detoxifies organic hydroperoxides, and its oxidized form (GSSG) are also excreted into bile. These organic compounds share the same molecular mechanism for their recognition and excretion into bile, that is, a conjugate-transporting ATPase called mul-

[1]First Department of Surgery, Nagoya University College of Medicine, Nagoya, Japan.
[2]Department of Biochemistry and Integrative Medical Biology, School of Medicine, Keio University, Tokyo, Japan.

tidrug resistance protein 2 (mrp2) (2, 3, 10). This transport ATPase is expressed in the hepatocellular membrane and facilitates the excretion of the organic conjugates into bile. The protein is not expressed in human Dubin–Johnson syndrome, which is therefore associated with an inherited hyperbilirubinemia caused by deficiency in the bilirubin excretion (8, 13). mrp2 serves as a determinant for biliary concentrations of the organic constituents and thus contributes to the generation of the osmotic driving force for bile formation, as well as other transporters such as the bile salt export pump, which represents the rate-controlling step for taurocholate excretion (20). However, mechanisms for regulation of the transporter function and their link to detoxification of noxious stressors and/or xenobiotics have not been fully investigated yet.

This study attempted to examine if such a cooperative link between the oxygenase-dependent enzymes and the transporter systems could function to regulate bile formation. Among by-products of the detoxification-associated oxygenase reaction, carbon monoxide (CO) has recently attracted great interest as an important protectant against hepatobiliary dysfunction (4, 25). We have shown that livers use CO derived from the HO reaction to relax sinusoids and thereby to guarantee ample blood supply under varied disease conditions, as well as physiologic circumstances (4, 16, 22, 25). The gas could also have the ability to alter bile formation through multiple mechanisms. Elimination of endogenous CO induces sinusoidal contraction through mechanisms involving soluble guanylate cyclase in hepatic stellate cells and induces bile acid-dependent choleresis (4, 9, 19). On the other hand, we have herein investigated effects of physiologically relevant concentrations of CO on bile formation and biliary constituents in perfused rat livers. To reveal the functional link between the gas and the ATP-dependent transporter, biliary responses upon CO exposure were compared between livers from normal rats and those from mrp2-lacking mutant rats. Results of the current study provided evidence that exogenously administered CO at inducible concentrations stimulates mrp2-dependent excretion of bilirubin-IXα and glutathione into bile, suggesting an important role of the HO-derived gas in regulation of the metabolism of the organic compounds.

MATERIALS AND METHODS

Animal preparation

Male Wistar and Sprague–Dawley rats and Eisai hyperbilirubinemia rats (EHBR) (280–300 g) were obtained from Nippon Biosupply Center Inc. (Tokyo, Japan) (2). All animals were allowed free access to laboratory chow and tap water, and were fasted 24 h when necessary. Protocols for the current experiments were approved according to the Institutional Guidelines for Animal Care and Experiments in Keio University School of Medicine. Rats were anesthetized intraperitoneally with pentobarbital sodium at 50 mg/kg. The livers underwent cannulation of the common bile duct with a PE-10 tube and were perfused *ex vivo* with hemoglobin-free and albumin-free Krebs–Ringer solution (pH 7.4, 37°C) gassed with carbogen according to our previous methods (19, 28). The perfusate contained 30 μmol/L sodium taurocholate and was pumped from the portal vein through the liver at a constant flow rate of 4.0 ml/min/g of liver weight under monitoring of the whole organ vascular resistance (25, 28). Bile was collected every 5 min throughout the experiments.

Bile constituents such as bile salts, phospholipids, glutathione, and potassium (K^+) and bicarbonate (HCO_3^-) ions were determined as described elsewhere (25, 28). We also determined biliary flux of bilirubin-IXα, the end product of HO-mediated heme degradation using enzyme-linked immunosorbent assay as described previously (28, 29). The primary antibody for this assay was monoclonal antibody 24G7, which recognizes both conjugated and unconjugated forms of bilirubin-IXα (4, 28).

Experimental protocols

After the 20-min perfusion for the stabilization, the Krebs–Ringer buffer containing the desired concentrations of CO (2.0–20 μmol/L) was perfused for 40 min transportally as described previously (11, 19). The concentrations of CO were measured in advance in samples collected from the portal inlet using myoglobin-assisted spectrophotometry according to our previous methods (4, 11). When necessary, the desired concentrations of tetraethylammonium (TEA), a potassium channel blocker, were perfused together with CO. In these experiments, the TEA perfusion was started simultaneously with the CO perfusion. After the 40-min observation period of the perfusion, the isolated perfused livers were snap-frozen by liquid nitrogen to determine tissue contents of cyclic GMP (cGMP) and glutathione according to previous methods (11, 21, 28).

Measurements of horseradish peroxidase (HRP) excretion into bile

The effects of CO on biliary excretion of HRP were examined to determine alterations in the paracellular and transcellular fractions of bile transport in the identical single-pass perfused liver described in the previous section. At 20 min after the initial perfusion with a desired concentration of CO, a bolus of 25 mg of HRP was injected over 1 min. Bile samples were collected every 2 min for 10 min, and then every 5 min until the end of experiments. The concentrations of HRP in the collected bile samples were determined spectrophotometrically by measuring the rate of oxidation of 4-aminoantipyrine at 510 nm using a 96-well microplate reader as described previously (14, 19).

Analyses of mrp2-dependent excretion rates of 5-carboxyfluorescein (CF) into bile

To examine the effects of CO on the function of mrp2 to excrete exogenously loaded organic anions, CF diacetate at 2 μmol/L was added to the perfusate containing 1.5 mmol/L probenecid, a potent blocker of the transporter (1, 13). This reagent can enter hepatocytes (23, 24) and is hydrolyzed by esterase into CF to be excreted into bile. After the 10-min loading of CF diacetate, the liver was perfused with the probenecid-free buffer to trigger the excretion of CF into bile. The bile was sampled through the PE-10 tube cannulated into

the common bile duct. The bile samples were deep-frozen until the fluorescence measurements were carried out using a 96-well multichannel fluorescence spectrophotometer. The measurements were performed under epi-illumination at 430 nm, the isosbestic wavelength of the dye that yields fluorescence at 510 nm without interference with pH values of the samples. The concentrations of CF in samples were calibrated with known concentrations of CF dissolved in phosphate-buffered saline. As seen later in Results, the decay of the dye concentrations appeared to fit a single exponential by the use of the conventional least-squares method; thus, biliary CF lifetimes were determined as the time constant (τ) of the exponential curve. This method also allowed us to determine the decay of the dye exclusion independently of the initial amounts of CF loaded into the perfused liver. When necessary, the buffer containing CO at varied concentrations was perfused from 20 min prior to the CF diacetate loading to the end of experiments. The values of τ were compared between the livers treated with or without CO.

RESULTS

CO increases the baseline bile output without altering the vascular resistance

Figure 1 illustrates temporal alterations in the baseline bile output of the isolated perfused livers of fed and fasted rats. As seen in Fig. 1A, in response to the perfusion with 4 μmol/L CO, livers of the fed rats exhibited a significant elevation of the basal bile output without showing any notable changes in the vascular resistance. Figure 1B illustrates net increases in the bile flux measured at 30 min (%ΔBile flux) as a function of the concentrations of CO in the perfusate. The peak of the choleretic response was attenuated by further increases in the CO concentrations, disappearing at >10 μmol/L almost completely. On the other hand, the choleretic response elicited by 4 μmol/L CO was not evident when rats were fasted overnight, consistent with our previous results obtained from livers of fasted rats (14). As choleretic responses by CO in livers of fed rats suggest an increase in bile constituents responsible for the osmotic driving force, concentrations and fluxes of bile salts and phospholipids were examined. As seen in Fig. 1C, concentrations of these constituents were modestly decreased, whereas fluxes of them were hardly changed as a result of choleresis upon the CO perfusion. These results indicated that the CO-elicited choleresis is not accompanied by elevated excretion of bile salts and phospholipids, suggesting the involvement of another compound to yield the osmotic driving force in this event.

CO stimulates biliary excretion of bilirubin-IXα and glutathione

In an attempt to determine biliary constituents responsible for CO-elicited choleresis, we determined concentrations and fluxes of bilirubin-IXα and glutathione, two major organic anions producing the osmotic driving force for bile formation. As seen in Fig. 2A, the biliary concentration and the flux of bilirubin-IXα increased by 1.5- and 2.0-fold, respectively, upon the administration of 4 μmol/L CO. Such an increase in the bilirubin excretion was reduced when the greater concentrations of CO were perfused, exhibiting a profile of the dose responses similar to that of bile output. Biliary excretion of glutathione to CO also exhibited a dose-response curve similar to that of bilirubin-IXα. These results suggested that these organic anions undergo significant condensation in the hepatobiliary compartment and serve as major bile constituents providing osmotic driving force for CO-dependent choleresis.

We compared responses in the livers of Wistar rats and EHBR, which genetically lack mrp2, the major organic anion transporter responsible for excretion of these compounds. As seen in Fig. 3A, livers of EHBR displayed a significant reduction of the basal bile output, being ~60% of the values measured in those of male Wistar rats. Concurrently with such a marked reduction of the basal bile output, the basal excretion of bilirubin-IXα and glutathione in EHBR livers was

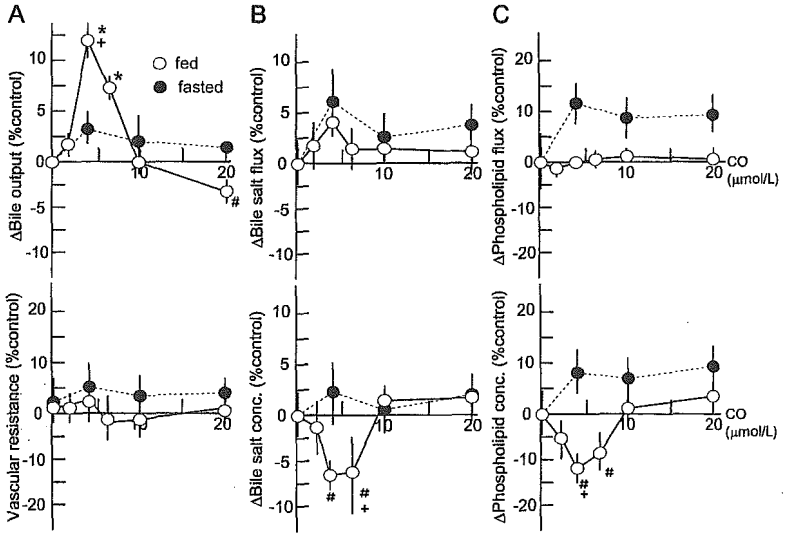

FIG. 1. Concentration-dependent effects of CO on bile output, vascular resistance, and biliary fluxes and concentrations of bile salts and phospholipids in perfused rat livers isolated from fed and fasted rats. Data were collected at 30 min after the start of the CO perfusion and indicate the means ± SE of more than six separate experiments. $*p < 0.05$, significantly increased versus the fed livers perfused without CO; $^{+}p < 0.05$, as compared with the values in fasted livers. $\#p < 0.05$, significantly decreased versus the fed livers perfused without CO.

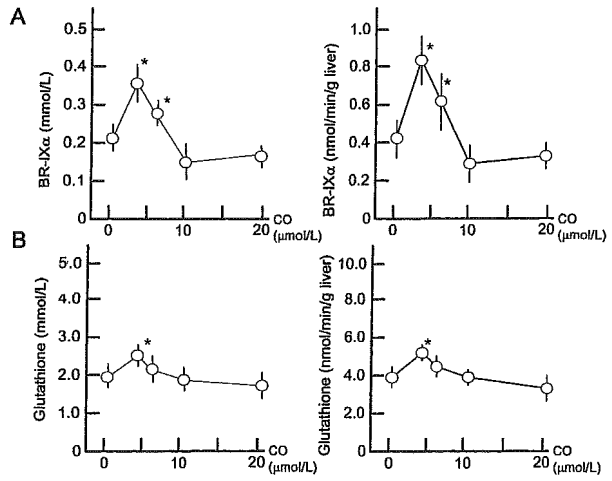

FIG. 2. Alterations in biliary concentrations and fluxes of bilirubin (BR)-IXα and glutathione by different concentrations of CO in perfused rat livers. Data were collected at 30 min after the start of the CO perfusion and indicate the means ± SE of more than six separate experiments. *$p < 0.05$, significantly increased versus the fed livers perfused without CO.

diminished almost completely. When 4 μmol/L CO was perfused, the EHBR livers did not exhibit any notable increase in excretion of these organic anions, being distinct from the responses elicited by the same concentration of CO in male Wistar rats. We also confirmed that the CO-induced choleresis was reproducible in the livers of male Sprague–Dawley rats (data not shown). These results suggest that the choleretic action of CO is operated specifically through mrp2-dependent mechanisms.

CO does not alter excretion of exogenous CF in perfused livers

The observation that CO stimulates mrp2-mediated excretion of organic anions in perfused livers led us to examine if mechanisms for this event involve the direct action of the gas on the function of the transporter. To address this possibility, rat livers were loaded with CF diacetate in the presence of 1.5 m*M* probenecid, an mrp2 inhibitor, and the biliary CF excretion after removal of the inhibitor was traced as a function of time for perfusion. As seen in Fig. 4, concentrations and fluxes of CF in bile samples were low at basal levels when the livers were perfused with the buffer containing probenecid. Upon its removal, the concentrations and fluxes of CF peaked at 10 min, and decreased with time, following a single exponential decay. Such a profile of the biliary CF excretion was unchanged when the livers were perfused with 4 μmol/L CO. The values of τ of the exponential decay of biliary CF concentrations were almost identical between the two groups, where those in the CO-untreated and -treated groups were 7.3 ± 0.4 min and 7.4 ± 0.4 min, respectively. These results suggest that CO does not directly stimulate function of mrp2 at least under the current experimental conditions.

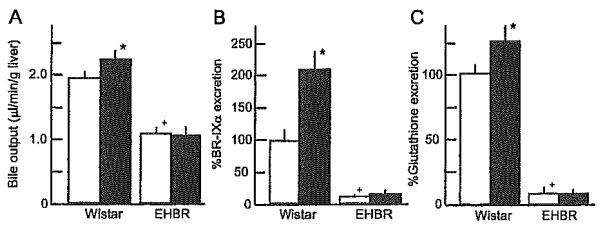

FIG. 3. Disappearance of CO-elicited increases in biliary excretion of bilirubin (BR)-IXα and glutathione and bile output in perfused livers isolated from EHBR. Data were collected at 30 min after the start of the CO perfusion at 4 μmol/L and indicate the means ± SE of more than six separate experiments. Open and filled columns indicate fed and fasted rats, respectively.

Blockade of potassium channels represses CO-elicited choleresis

To further determine mechanisms by which CO stimulates excretion of bilirubin and glutathione, we examined the effects of TEA, a blocker for a wide spectrum of potassium channels, on bile output and constituents such as K^+ and HCO_3^-, because the gas has been known to increase the opening probability of the channels to hyperpolarize cells (17). As seen in Fig. 5, perfusion of CO at 4 μmol/L significantly increased the fluxes of HCO_3^-. These changes were attenuated by coperfusion of TEA in a dose-dependent manner. In these experiments, the whole organ vascular resistance among the groups did not differ, suggesting that the biliary responses modified by TEA do not result from its action on

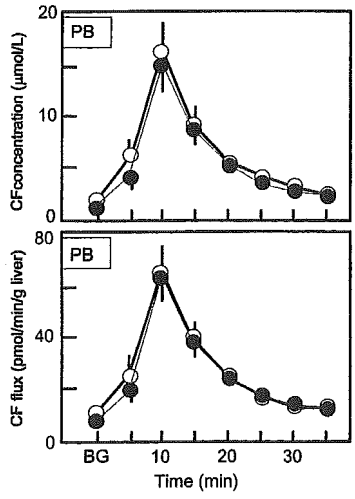

FIG. 4. Temporal alterations in biliary excretion of CF in the presence or absence of 4 μmol/L CO in the perfused rat livers. PB, 1.5 mmol/L probenecid, an inhibitor of mrp2. Note that time courses of the dye exclusion in the control and CO-treated groups are almost identical to each other and those after reaching the peaks follow a single exponential. The time constants (τ) were not statistically different between the two groups. Values are means ± SE of more than six separate experiments. Open and filled circles indicate the control and CO-treated groups, respectively.

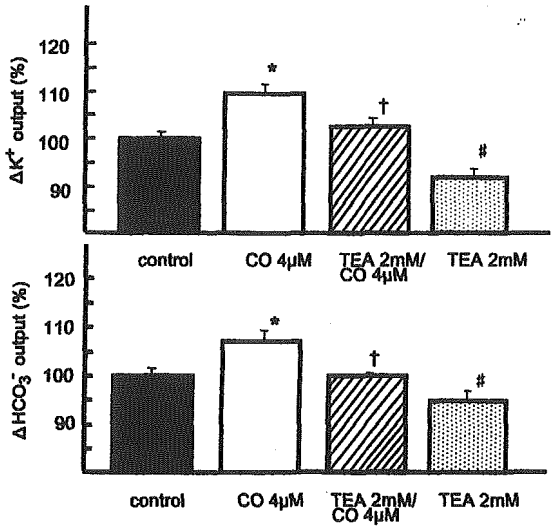

FIG. 5. Effects of TEA on the CO-elicited increases in fluxes of potassium and bicarbonate ions in perfused rat livers. Data were collected from livers perfused with or without 4 μmol/L CO for 30 min, and indicate the means ± SE of more than six experiments. $^*p < 0.05$, significantly increased versus the fed control livers; $^\dagger p < 0.05$, as compared with the values in fed livers perfused with 4 μmol/L CO; $\#p < 0.05$, significantly decreased versus the fed control livers.

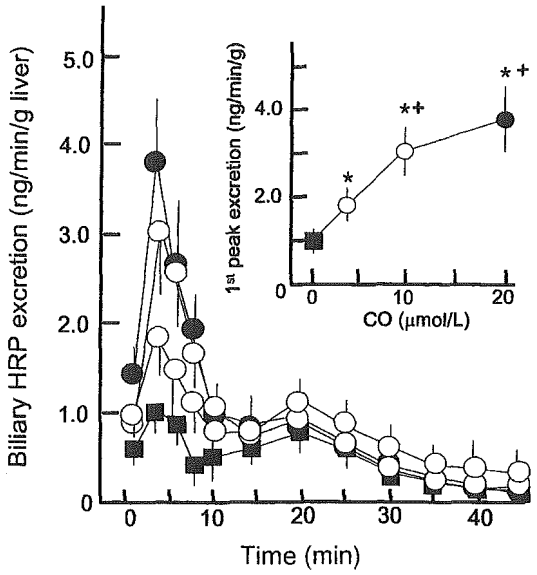

FIG. 6. Differences in time course of biliary HRP excretion in the perfused livers of fed rats. At 20 min after the initial perfusion with desired concentrations of CO, a bolus of HRP (25 mg) was injected. The initial peak at 4 min after injection of HRP reflects paracellular transport of portally injected HRP. Values are means ± SE of more than five experiments. **Inset:** Relationship between CO concentrations and heights of the first peak at 4 min after the injection of HRP. Note that the height of the initial peak increases with elevated concentrations of CO in the perfusate, and reaches the maximum level with 20 mmol/L. Filled square and open, shaded, and filled circles denote CO concentrations of 0, 4, 10, and 20 μmol/L, respectively. $^*p < 0.05$, significantly increased versus the CO-untreated group; $^\dagger p < 0.05$, significantly increased versus the 4 μmol/L CO-treated group.

the vascular system, but from that on nonvascular components such as hepatocytes and/or the biliary system. Collectively, the stimulatory action of CO on potassium channels appeared to be involved in mechanisms for choleretic responses.

The choleretic response induced by 4 μmol/L CO did not coincide with an increase in tissue contents of cGMP. On the other hand, the perfusion with CO at concentrations of >10 μmol/L induced modest, but significant, elevation of the cGMP contents in the liver (data not shown). As mentioned in the previous section, such concentrations of CO did not induce choleresis and rather elicited a repression of the bile output comparable to the level measured in the absence of the gas. These results suggest that the CO-induced choleretic response is an event occurring independently of its effect to activate soluble guanylate cyclase.

Excess CO increases paracellular junctional permeability and cancels choleresis

The observation that CO at >4 μmol/L blunts the choleretic responses led us to examine if such concentrations of the gas could reduce concentrations of biliary constituents and result in a decrease in the osmotic driving force for bile formation. Figure 6 illustrates differences in the time course of biliary HRP excretion in the perfused livers of fed rats. Previous studies demonstrated that the initial peak at 4 min and the second one at 20 min after completion of the transportal HRP injection reflect paracellular and transcellular transport of portally injected HRP (14, 19). As seen, the height of the initial peak increased with elevated concentrations of CO in the perfusate, and reached the maximum level with 20 μmol/L by fourfold versus the control values. These results suggest that the paracellular permeability increased in response to the gas administration even in fed rats, consistent with our previous data collected from fasted rats.

DISCUSSION

The current study demonstrated that CO at micromolar concentrations has the ability to induce choleresis and to stimulate biliary excretion of glutathione and bilirubin-IXα in perfused livers of fed rats. Such an action of CO appears to result from cGMP-independent mechanisms and to depend on TEA-sensitive potassium channels. Quantitative analyses of bile constituents revealed that glutathione and/or bilirubin-IXα appear to be major components generating osmotic driving force for bile formation. A range of CO concentrations eliciting choleresis is 4–6 μmol/L in the perfusate; such concentrations could occur under disease conditions such as endotoxemia as a consequence of stress-induced HO-1 induction and subsequent degradation of heme in the liver (11). As the biliary excretion of the aforementioned organic anions is an important process of xeno-

biotic detoxification under varied stress conditions, such an ability of stress-inducible levels of CO could serve as an important fail-safe mechanism to guarantee bile formation for excretion of detoxified metabolites.

The effect of gaseous mediators on biliary excretion was previously reported by Trauner *et al.* (26), where a stimulatory effect of nitric oxide (NO) on biliary excretion of glutathione was suggested in a similar model using isolated rat livers perfused with the taurocholate-free oxygenated buffer. In this report, the liver perfused with high concentrations of NO donors exhibited a dose-dependent choleresis in parallel with an elevation of glutathione. The mechanisms of this event are unlikely to involve cGMP-mediated processes because administration of a membrane-permeable cGMP analogue did not increase biliary excretion of glutathione. Although such effects of NO appear to be similar to those of CO, the current finding provides several unique features of this CO-mediated event. First, a novel role of CO in regulating biliary excretion of bilirubin is revealed for the first time. As we reported previously, physiologic concentrations of bile salts (*e.g.,* 30 μmol/L taurocholate) are necessary to guarantee directional excretion of bilirubin-IXα from hepatocytes into bile canaliculi (29). As livers were not perfused with bile salts in the previous study, the excretion of bilirubin was not able to be assessed. Second, the current results demonstrated that CO-mediated choleresis is notable only in livers of fed rats, but not in those of fasted ones, where the osmotic driving force for bile formation by glutathione is not sufficient because of its reduced contents in the liver. Although it has been known that hepatic glutathione concentration of fed rats is higher than that of fasted ones (6, 18, 26, 27), feeding effects on CO-mediated choleresis have not been assessed in these studies. Third, effects of CO on biliary excretion of organic anions occur in a concentration-specific manner, and excess concentrations of the gas cause a repression of the responses. The mechanisms for repression of bile output by excess CO appear to involve reduced concentrations of the organic anions in bile due to the increase in paracellular junctional permeability, suggested in Fig. 5 of the current study, as well as in our previous report (14).

These lines of evidence led us to further examine mechanisms by which CO regulates excretion of bilirubin and glutathione into bile. As these two organic anions were present at millimolar levels in bile and constitute a major osmotic driving force for bile formation, we examined if the function of mrp2, the anion transporter for these compounds, could be regulated by CO. The current study confirmed the requirement of mrp2 in the CO-mediated choleresis using EHBR. However, results collected from analyses of biliary exclusion of exogenously applied CF, a fluorescent organic anion excreted by mrp2, did not support a notion that CO directly stimulates function of the organic anion transporter. On the other hand, the data showing repressive effects of TEA suggest that potassium channels could be a potentially important target of CO as also documented in previous observations (7). Thus, the functional link between the ion channels and mrp2 should be examined further to reveal the entire mechanisms for the CO-mediated choleresis and enhanced excretion of the organic anions.

Collectively with previous reports (11, 12, 16), the current results suggest the whole picture of HO-mediated protective mechanisms against noxious stimuli to the liver that is schematized in Fig. 7. Using the rat experimental model of endotoxemia, we have shown that the stimulated liver increases degradation of heme through at least two mechanisms: an increase in the substrate and an induction of HO-1. When such livers are exposed to methemoglobin, the heme derived from senescent erythrocytes or from hemolysis in circulation, the heme serves as a substrate for both HO-1 and HO-2 in hepatocytes and facilitates endogenous CO generation (11). Furthermore, cell damages could cause denaturation of heme proteins and provide free heme to be degraded by the HO (15). As a result, the livers are exposed to sufficient amounts of CO that could stimulate sinusoidal flow and bile formation. Under these circumstances, our results showed that overproduced CO keeps sinusoids in relaxing states through mechanisms involving its inhibitory actions on cytochrome P450 monooxygenases (11). In addition to such HO-mediated protective mechanisms, the current study raised the possibility that stress-inducible levels of CO could directly stimulate bile formation by facilitating excretion of glutathione and bilirubin through mechanisms independent of its cGMP-independent vasorelaxing actions. In this context, the current study shed light on a novel action of CO on biliary excretion of the heme-degrading pigment, serving as a cooperator standing behind the HO reaction to facilitate hepatic heme detoxification. At present, it is unknown whether the direct choleretic action of CO operated by cGMP-independent pathways could involve alterations in cytochrome P450-derived eicosanoids in hepatocytes. However, such a possibility could be supported by our previous studies suggesting that micromolar levels of CO contribute to maintain stroke volume of bile canalicular contraction in cultured hepatocyte couplets, where the gas appears to inhibit the monooxygenase activities and thereby modulates calcium-dependent contrac-

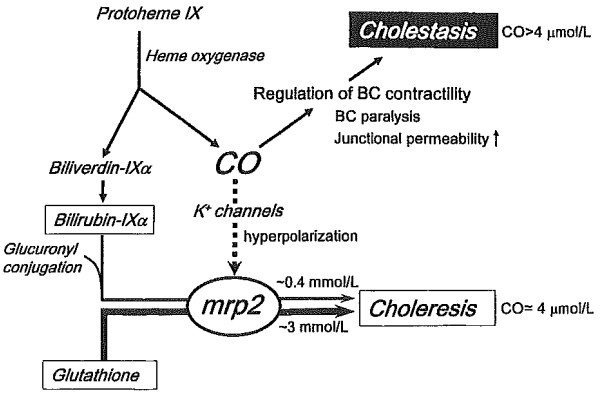

FIG. 7. Possible mechanisms involving CO-mediated choleresis. Stress-inducible CO (~4 μmol/L) could stimulate bile formation by facilitating mrp2-dependent excretion of glutathione, a major component for yielding osmotic driving force for bile formation, and bilirubin-IXα, the end product of heme degradation. CO increases conductance of potassium channels and hyperpolarizes membrane that could help efflux of organic anions through mrp2. Greater concentrations of CO could reduce this choleretic response through multiple mechanisms involving impaired bile canalicular (BC) contraction and increased paracellular junctional permeability.

tion processes (21). Further investigation is necessary to examine whether such a mechanism is involved in the regulation of mrp2 function in hepatocytes.

ACKNOWLEDGMENTS

The authors thank Hitomi Irisawa for expert technical support in measurements of bile constituents. This study was supported by Advanced Medical Technology in Health and Sciences Research Grants from Ministry of Health and Welfare in Japan, from Grant-in-Aid for Creative Scientific Research (13GS0015), and from 21st Century Center-of-Excellence Program from Ministry of Education, Sciences and Technology.

ABBREVIATIONS

CF, 5-carboxyfluorescein; cGMP, cyclic GMP; CO, carbon monoxide; EHBR, Eisai hyperbilirubinemia rat(s); HO, heme oxygenase; HRP, horseradish peroxidase; mrp2, multidrug resistance protein 2; NO, nitric oxide; TEA, tetraethylammonium.

REFERENCES

1. Courtois A, Payen L, Lagadic D, Guillouzo A, and Fardel O. Evidence for a multidrug resistance-associated protein 1 (MRP1)-related transport system in cultured rat liver biliary epithelial cells. *Life Sci* 64: 763–774, 1999.
2. Fernandez-Checa JC, Takikawa H, Horie T, Ookhtens M, and Kaplowitz N. Canalicular transport of reduced glutathione in normal and mutant Eisai hyperbilirubinemic rats. *J Biol Chem* 267: 1667–1673, 1992.
3. Gatmaitan ZC and Arias IM. ATP-dependent transport systems in the canalicular membrane of the hepatocyte. *Physiol Rev* 75: 261–275, 1995.
4. Goda N, Suzuki K, Naito M, Takeoka S, Tsuchida E, Ishimura Y, Tamatani T, and Suematsu M. Distribution of heme oxygenase isoforms in rat liver. Topographic basis for carbon monoxide-mediated microvascular relaxation. *J Clin Invest* 101: 604–612, 1998.
5. Hayashi S, Takamiya R, Yamaguchi T, Matsumoto K, Tojo SJ, Tamatani T, Kitajima M, Makino N, Ishimura Y, and Suematsu M. Induction of heme oxygenase-1 suppresses venular leukocyte adhesion elicited by oxidative stress: role of bilirubin generated by the enzyme. *Circ Res* 85: 663–671, 1999.
6. Isaacs J and Binkley F. Glutathione dependent control of protein disulfide-sulfhydryl content by subcellular fractions of hepatic tissue. *Biochim Biophys Acta* 497: 192–204, 1977.
7. Kajimura M, Goda N, and Suematsu M. Organ design for generation and reception of CO: lessons from the liver. *Antioxid Redox Signal* 4: 633–637, 2002.
8. Kartenbeck J, Leuschner U, Mayer R, and Keppler D. Absence of the canalicular isoform of the MRP gene-encoded conjugate export pump from the hepatocytes in Dubin–Johnson syndrome. *Hepatology* 23: 1061–1066, 1996.
9. Kashiwagi S, Suematsu M, Wakabayashi Y, Kawada N, Tachibana M, Koizumi A, Inoue M, Ishimura Y, and Kaneko A. Electrophysiological characterization of cultured hepatic stellate cells in rats. *Am J Physiol* 272: G742–G750, 1997.
10. Keppler D and Konig J. Hepatic canalicular membrane 5: expression and localization of the conjugate export pump encoded by the MRP2 (cMRP/cMOAT) gene in liver. *FASEB J* 11: 509–516, 1997.
11. Kyokane T, Norimizu S, Taniai H, Yamaguchi T, Takeoka S, Tsuchida E, Naito M, Nimura Y, Ishimura Y, and Suematsu M. Carbon monoxide from heme catabolism protects against hepatobiliary dysfunction in endotoxin-treated rat liver. *Gastroenterology* 120: 1227–1240, 2001.
12. Makino N, Suematsu M, Sugiura Y, Morikawa H, Shiomi S, Goda N, Sano T, Nimura Y, Sugimachi K, and Ishimura Y. Altered expression of heme oxygenase-1 in the livers of patients with portal hypertensive diseases. *Hepatology* 33: 32–42, 2001.
13. Mor-Cohen R, Zivelin A, Rosenberg N, Shani M, Muallem S, and Seligsohn U. Identification and functional analysis of two novel mutations in the multidrug resistance protein 2 gene in Israeli patients with Dubin–Johnson syndrome. *J Biol Chem* 276: 36923–36930, 2001.
14. Mori M, Suematsu M, Kyokane T, Sano T, Suzuki H, Yamaguchi T, Ishimura Y, and Ishii H. Carbon monoxide-mediated alterations in paracellular permeability and vesicular transport in acetaminophen-treated perfused rat liver. *Hepatology* 30: 160–168, 1999.
15. Ortiz de Montellano PR and Coreia MA. Suicidal destruction of cytochrome P-450 during oxidative drug metabolism. *Annu Rev Pharmacol Toxicol* 23: 481–503, 1983.
16. Pannen BH, Kohler N, Hole B, Bauer M, Clemens MG, and Geiger KK. Protective role of endogenous carbon monoxide in hepatic microcirculatory dysfunction after hemorrhagic shock in rats. *J Clin Invest* 102: 1220–1228, 1998.
17. Rich A, Farrugia G, and Rae JL. Carbon monoxide stimulates a potassium-selective current in rabbit corneal epithelial cells. *Am J Physiol* 267: C435–C442, 1994.
18. Robinson MK, Rustum RR, Chambers EA, Rounds JD, Wilmore DW, and Jacobs DO. Starvation enhances hepatic free radical release following endotoxemia. *J Surg Res* 69: 325–330, 1997.
19. Sano T, Shiomi M, Wakabayashi Y, Shinoda Y, Goda N, Yamaguchi T, Nimura Y, Ishimura Y, and Suematsu M. Endogenous carbon monoxide suppression stimulates bile acid-dependent biliary transport in perfused rat liver. *Am J Physiol* 272: G1268–G1275, 1997.
20. Schmitt M, Kubitz R, Lizun S, Wettstein M, and Haussinger D. Regulation of the dynamic localization of the rat Bsep gene-encoded bile salt export pump by anisoosmolarity. *Hepatology* 33: 509–518, 2001.
21. Shinoda Y, Suematsu M, Wakabayashi Y, Suzuki T, Goda N, Saito S, Yamaguchi T, and Ishimura Y. Carbon monoxide as a regulator of bile canalicular contractility in cultured rat hepatocytes. *Hepatology* 28: 286–295, 1998.
22. Suematsu M and Ishimura Y. The heme oxygenase–carbon monoxide system: a regulator of hepatobiliary function. *Hepatology* 31: 3–6, 2000.

23. Suematsu M, Suzuki H, Ishii H, Kato S, Yanagisawa T, Asako H, Suzuki M, and Tsuchiya M. Early midzonal oxidative stress preceding cell death in hypoperfused rat liver. *Gastroenterology* 103: 994–1001, 1992.
24. Suematsu M, Tamatani T, Delano FA, Miyasaka M, Forrest M, Suzuki H, and Schmid-Schönbein GW. Microvascular oxidative stress preceding leukocyte activation elicited by in vivo nitric oxide suppression. *Am J Physiol* 266: H2410–H2415, 1994.
25. Suematsu M, Goda N, Sano T, Kashiwagi S, Egawa T, Shinoda Y, and Ishimura Y. Carbon monoxide: an endogenous modulator of sinusoidal tone in the perfused rat liver. *J Clin Invest* 96: 2431–2437, 1995.
26. Trauner M, Nathanson MH, Mennone A, Rydberg SA, and Boyer JL. Nitric oxide donors stimulate bile flow and glutathione disulfide excretion independent of guanosine 3′,5′-cyclic monophosphate in the isolated perfused rat liver. *Hepatology* 25: 263–269, 1997.
27. Vendemiale G, Grattagliano I, Caraceni P, Caraccio G, Domenicali M, Dall'Agata M, Trevisani F, Guerrieri F, Bernardi M, and Altomare E. Mitochondrial oxidative injury and energy metabolism alteration in rat fatty liver: effect of the nutritional status. *Hepatology* 33: 808–815, 2001.
28. Wakabayashi Y, Takamiya R, Mizuki A, Kyokane T, Goda N, Yamaguchi T, Takeoka S, Tsuchida E, Suematsu M, and Ishimura Y. Carbon monoxide overproduced by heme oxygenase-1 causes a reduction of vascular resistance in perfused rat liver. *Am J Physiol* 277: G1088–G1096, 1999.
29. Yamaguchi T, Wakabayashi Y, Tanaka M, Sano T, Ishikawa H, Nakajima H, Suematsu M, and Ishimura Y. Taurocholate induces directional excretion of bilirubin into bile in perfused rat liver. *Am J Physiol* 270: G1028–G1032, 1996.

Address reprint requests to:
Makoto Suematsu, M.D., Ph.D.
Professor and Chair
Department of Biochemistry and Integrative Medical Biology
School of Medicine, Keio University
35 Shinanomachi, Shinjuku-ku
Tokyo 160-8582, Japan

E-mail: msuem@sc.itc.keio.ac.jp

Received for publication January 10, 2003; accepted March 19, 2003.

ANTIOXIDANTS & REDOX SIGNALING
Volume 5, Number 4, 2003

Forum Review

Mechanistic Probing of Gaseous Signal Transduction in Microcirculation

MAKOTO SUEMATSU, KAZUHIRO SUGANUMA, and SATOSHI KASHIWAGI

ABSTRACT

Nitric oxide (NO) and carbon monoxide (CO) serve as activators of soluble guanylate cyclase (sGC) *in vitro*, and the latter serves as a microvascular relaxant for the liver, a major organ for heme oxygenase-dependent heme degradation and gas generation. Another important determinant of local sGC activities is superoxide anion, which scavenges NO and/or activates sGC directly. Altered bioavailability of the oxygen-derived species and its functional outcomes remain unknown, because information on amounts and distribution of these molecules has hardly been examined *in vivo*. Our recent studies provided evidence for such complex actions of multiple gases *in vivo*. Intravital visualization of NO in microcirculation revealed that two distinct sources, NO synthase-1 and -3, play a major role in the maintenance of NO in arteriolar and venular walls, respectively. Besides its vasorelaxing action in the hepatic microcirculation, CO could induce vasoconstriction in the resistant artery where NO is abundantly available; systemic blood pressure was elevated in transgenic mice overexpressing heme oxygenase-1 site-specifically in vascular smooth muscle cells. Such a relationship between the gases has also been demonstrated by mechanistic bioprobing of sGC function using novel monoclonal antibodies. This article aims to provide an overview of advances in visual assessment of the generation and reception of oxygen-derived gaseous mediators *in vivo*. *Antioxid. Redox Signal.* 5, 485–492.

BACKGROUND

MOLECULAR OXYGEN functions primarily as a terminal acceptor of electrons on mitochondrial electron transport. Most of the oxygen consumed in this process is reduced to generate water through the reaction of cytochrome oxidase. Only a small fraction of oxygen is used to generate compounds that exert potent biological actions; such compounds include prostaglandins, oxidized phospholipids, reactive oxygen species (ROS) such as superoxide, hydrogen peroxide, and hydroxyl radical, and gaseous molecules such as nitric oxide (NO) and carbon monoxide (CO) (Fig. 1) (25). Amounts and localization of all these species depend on supply of molecular oxygen and expression of the generator enzymes, and their functional outcomes after various intracellular signaling cascades were examined by the proximity of receptor proteins to the gas-generating systems. However, such topographic information has not been available because of technical limitations to detect behavior of these small molecules as discernible molecular entities and to visualize functional alterations in the gas signal transducers in vivo. We have attempted to overcome such difficulties to visually prove mechanisms for gaseous signal transduction in cellular components involving endothelial cells, vascular smooth muscle cells, pericytes, mast cells, and platelets and leukocytes in microcirculation. This article for the Forum aims to summarize our methods that have shed new light on mechanisms whereby multiple gases execute their ability to fine-tune functions of microcirculation.

Department of Biochemistry and Integrative Medical Biology, School of Medicine, Keio University, Tokyo 160–8582, Japan.